PHYSICAL REVIEW B VOLUME 23, NUMBER 10 15 MAY 1981

Deep-level optical spectroscopy in GaAs

A. Chantre
Centre National d'Etudes des Télécommunications, Centre de Microélectronique de Grenoble, 38240 Grenoble, France

G. Vincent
Institut National des Sciences Appliquées, Laboratoire de Physique de la Matière, 69621 Lyon, France

D. Bois
Centre National d'Etudes des Télécommunications, Centre de Microélectronique de Grenoble, 38240 Grenoble, France

(Received 5 February 1980)

An experimental method which we call deep-level optical spectroscopy (DLOS) is described. It is based on photostimulated capacitance transients measurements after electrical, thermal, or optical excitation of the sample, i.e., a diode. This technique provides the spectral distribution of both $\sigma_n^0(h\nu)$ and $\sigma_p^0(h\nu)$, the optical cross sections for the transitions between a deep-level and the conduction and valence bands. Besides its sensitivity, DLOS is selective in the double sense that $\sigma_n^0(h\nu)$ and $\sigma_p^0(h\nu)$ are unambiguously separated, and that the signals due to different traps can be resolved from one another. As a result, the $\sigma^0(h\nu)$ spectra are measured from their threshold up to the energy gap of the semiconductor, over a generally large temperature range. In addition, the straightforward coupling of DLOS with deep-level transient spectroscopy allows a clear identification of the optical spectra with known levels and the simultaneous determination of both thermal and optical properties for each defect. This experimental method has been used to analyze the most commonly observed deep levels in GaAs. For the well known "O" level, a comprehensive analysis of the results obtained through other techniques (as reported in the literature) is given, to compare with our DLOS data. The spectral shape of all $\sigma_n^0(h\nu)$ curves appears to be strongly related to the density-of-states distribution in the conduction band, i.e., transitions towards Γ, L, and X minima of this band are generally well resolved; this is a unique feature of DLOS. A simple theoretical model is proposed to take advantage of these newly available experimental data and to explain the sharpness of the $\sigma_p^0(h\nu)$ curves, as compared with, e.g., Lucovsky's model. Phonon coupling is taken into account. A good fit of the DLOS results is obtained with a small number of adjustable parameters: the deep-level envelope wave function extent (in the δ-potential approximation), the relative transition probabilities to the various conduction-band minima, and the Franck-Condon parameter. The values thus obtained for these physical parameters are discussed, and finally, all results concerning each trap are summarized on a configuration coordinate diagram.

I. INTRODUCTION

Our present knowledge about deep levels in semiconducting materials is often restricted to experimental measurements of thermal ionization energies and free-carrier-capture cross sections. Even more, some problems still subsist in the determination of these physical quantities, so that one now prefers to speak of the signature of a deep level, that is, the crude thermal emission rate versus temperature curve.[1] Indeed, such a phenomenological analysis is very useful for classifying and labeling the levels in a given material, but it must be followed by physical studies, if one wants to really understand the deep-level properties. In that view, several experimental approaches must be used: Thermal measurements, while providing a good background, cannot be used alone. As is generally the case in atomic or molecular physics, optical measurements are among the most powerful tools. In particular, the spectral distributions of the optical cross sections $\sigma_n^0(h\nu)$ and $\sigma_p^0(h\nu)$ for the transitions between a localized level and the conduction and valence bands are of prime interest. They provide information, not only about the ionization energies of the levels, but also about the electron-phonon interaction and temperature dependence of the levels, i.e., about their relations with each band. Since these cross sections are directly related to the matrix elements coupling the deep-level wave function to either the conduction or valence band Bloch free-carrier wave functions, they can constitute a very good test for theoretical calculations concerning deep levels. These theoretical works being now under progress, such experimental informations are strongly desirable. In addition, the knowledge of the optical cross sections can also be of great interest for an unambiguous interpretation of some other experimental results, such as pressure effects, for example.[2] And let us note that optical spectroscopy is the unique way of studying very deep levels in large gap materials, i.e., when thermal emission is not possible in the experimentally available temperature range.

Several experimental techniques can be used to investigate the optical properties of deep levels: mainly optical absorption, luminescence, photoconductivity or photovoltage, and photocapacitance. These techniques can be compared according to four points: their sensitivity, their selectivity when several deep levels are present in a given sample, which is the common case, their ability to provide an independent analysis of the transitions with the conduction and valence bands, and the data processing which is necessary to extract the results. Extrinsic optical absorption measurements, together with luminescence, gave first evidence for strong phonon coupling for deep levels in GaAs.[3] One of the main drawbacks of this technique is certainly its poor sensitivity. Generally, very thick samples (a few millimeters) are required; therefore it cannot be used to study the best controlled and purest materials, i.e., epitaxial layers. Moreover, optical absorption is not selective and generally does not provide both $\sigma_n^0(h\nu)$ and $\sigma_p^0(h\nu)$ cross sections for a deep level; such a determination would require to prepare n- and p-type samples with exactly the same deep levels. The main interest of optical absorption is that experimental data are easily interpreted without any calculations and possible experimental errors. It can thus be used when one deep level only is present, with a large concentration, in a bulk material: chromium in GaAs, for example.[4-5] The sensitivity and capabilities of luminescence measurements are always limited by the competition between the different possible radiative and nonradiative mechanisms. Moreover, the emission lines do not provide information about the spectral shape of the optical cross sections because only near-edge energy states are involved. This has, in turn, an advantage: These lines are not a convolution of free-carrier density of states and phonon-coupling effects; thus vibrational states can be directly observed, in particular, zero-phonon lines.[6,7] As far as radiative deep levels are concerned, however, photoluminescence excitation and quenching spectra measurements have proven to be a very powerful means of investigating the optical cross sections, down to the lowest temperatures.[8,9] Photoconductivity is a very sensitive tool. Before the lively development brought about by Grimmeiss,[10] i.e., constant photocurrent technique, the experimental results were difficult to interpret because the photocurrent is a complex function of the optical emission rates and the carrier population on the deep levels. However, this last technique is still restricted to insulating, i.e., compensated, samples and, as optical absorption, it does not provide both $\sigma_n^0(h\nu)$ and $\sigma_p^0(h\nu)$ cross sections independently, especially in the case of very deep levels. Even more, if the Fermi level is not known precisely, as frequently occurs in semiinsulating samples, one never knows precisely which of the two cross sections is actually under measurement.[11] Moreover, photoconductivity is not selective. All this leads to a difficult and often ambiguous data treatment to extract the characteristics of one deep level. One common feature of all the preceding techniques is that they do not allow simultaneous measurements of both thermal and optical characteristics of the traps, which would yield a clear indentification of the investigated levels.

In that view, photocapacitance appears to be a more powerful technique, because both the samples (Schottky barriers or junctions) and the measurement system are the same as those used for the thermal spectroscopy of deep levels. However, steady-state photocapacitance, as pioneered by Furukawa[12] and very often used,[13-16] or its recent improvement by White,[17] who uses a two-beam technique, does not make use of this potential advantage. These methods only provide the optical ionization energies of the levels. The determination of the spectral shape of the optical cross sections implies photocapacitance transients analysis as a function of photon energy; this is a very powerful but tedious method because point-by-point measurements and heavy data treatments are required.[18,19] Moreover, it remains not selective.

Let us compare this situation with that of thermally-induced capacitance transients. The same difficulties were arising until Lang[20] proposed to use a correlation technique to simplify the data processing, and therefore to make a real spectroscopy of the deep traps in a material. This deep-level transient spectroscopy (DLTS) technique has been widely used in the last few years[21-24] and thus proven its usefulness. Similar progress has not been made until now for optical measurements because of two main differences: (i) the photon energy dependence of optically induced emission of carriers is not as simple as that of thermally induced emission, which is always an exponential function of temperature; (ii) both optical cross sections σ_n^0 and σ_p^0 are generally involved at a given energy, while in the case of thermal emission only one emission term has to be considered. Therefore a two-gate, or equivalent, correlation technique cannot be used.

It is the purpose of this paper to discuss a transient photocapacitance technique which allows a true deep-level optical spectroscopy (DLOS), i.e., direct unambiguous independent measurement of both $\sigma_n^0(h\nu)$ and $\sigma_p^0(h\nu)$ cross sections over a large photon energy range with a very good sensitivity, and with selectivity when several deep levels are present in a given material. Although its physical principle was already known,[25,26] this method has never been extensively used until now. DLOS requires an experimental setup which is very similar to that used for DLTS (which can be understood here as deep-level thermal spectroscopy), so that both thermal and optical spectroscopies can be performed on the same sample. As a result, DLOS spectra can be quite easily associated to deep levels identified through their thermal signatures. This allows us to take advantage of the large amount of work made on deep levels in semiconductors using DLTS.

We have applied this technique to the main traps in GaAs; the results are presented in Sec. II. In Sec. III, we give a comparison with data previously reported in the literature and obtained through other techniques to demonstrate the validity of DLOS. Finally, in Sec. IV the results are discussed with respect to theoretical models for optical cross sections.

II. DEEP-LEVEL OPTICAL SPECTROSCOPY: PRINCIPLE AND RESULTS

A. Principle

When photons are sent into the depletion region of a junction, the deep-level occupancy can be changed by the optically induced emission of carriers, leading to a change of the capacitance of the junction. This is the basic idea of either steady-state or transient photocapacitance measurements. If temperature is low enough so that thermal release of trapped carriers can be neglected, the evolution of the occupancy of the level under illumination is given by the classical differential equation

$$\frac{dn_t}{dt} = -\sigma_n^0 \Phi n_t + \sigma_p^0 \Phi p_t , \tag{2.1}$$

where n_t and $p_t = N_t - n_t$ are the concentrations of electrons and holes trapped on the level, σ_n^0 and σ_p^0 the optical cross sections for the emission of electrons in the conduction band and holes in the valence band, respectively, and Φ is the intensity of the incident light.

So far, this relation has been used in two ways. The first one, proposed by Sah,[25] has been to study the time constant τ^0 of the capacitance transient corresponding to Eq. (2.1):

$$\tau^0 = (\sigma_n^0 \Phi + \sigma_p^0 \Phi)^{-1} . \tag{2.2}$$

Equation (2.2) shows that this time constant is related to the sum of the two optical cross sections. Thus this method can be used in a simple way only when one of the two terms is negligible. This arises for certain photon energies when the levels are far from the middle of the band gap[18,19] and in some very peculiar cases, such as the DX center in $Ga_{1-x}Al_xAs$, for which $\sigma_p^0 = 0$ because of a very large lattice relaxation.[27,28] Anyway, the data processing is tedious; very often one uses only steady-state measurements, i.e., Eq. (2.1) in the limit $t \to \infty$:

$$(n_t)_\infty = N_t \frac{\sigma_p^0}{\sigma_n^0 + \sigma_p^0} . \tag{2.3}$$

Again, the two cross sections are mixed, so that it is impossible to deduce $\sigma_n^0(h\nu)$ and $\sigma_p^0(h\nu)$. Moreover, as τ^0 can be large (several minutes), it is difficult to reach the steady-state condition. So a classical photocapacitance spectrum, obtained by continuously recording the capacitance as a function of photon energy $h\nu$, is a complex function of both cross sections and the $h\nu$-sweeping rate. It can be used only for a rapid qualitative characterization of a sample. The introduction of a second high intensity light beam, as pioneered by White,[17] avoids the trouble due to long time constants. In order to increase the resolution of their method, the authors propose to measure the derivative of the capacitance change while the photon energy is scanned (double source differentiated photocapacitance, DSDP). However, this does not avoid the trouble rising from the mixing between the $\sigma_n^0(h\nu)$ and $\sigma_p^0(h\nu)$ spectra, and furthermore, the derivation does not simplify the interpretation of the results.

The main feature of the proposed method is to use the opposite limiting case, i.e., $t \to 0$.[26,29,30] Indeed, at time $t = 0$, Eq. (2.1) can be simplified by choosing an initial condition such that only one of the two terms remains.

(i) If, at time $t = 0$, all the centers are filled with electrons, $n_t(0) = N_t$ and $p_t(0) = 0$, Eq. (2.1) becomes

$$\left(\frac{dn_t}{dt}\right)_0 = -\sigma_n^0 \Phi N_t , \tag{2.4}$$

N_t being a constant and $\Phi(h\nu)$ given by a previous calibration of the monochromator output; the $\sigma_n^0(h\nu)$ spectrum can be obtained by measuring the initial derivative of the capacitance transient $[(d\Delta C/dt)_0 \propto (dn_t/dt)_0]$ just after the beginning of the illumination.

(ii) On the other hand if, at time $t = 0$, all the centers are filled with holes, $p_t(0) = N_t$ and $n_t(0) = 0$, then the same measurement will lead to the $\sigma_p^0(h\nu)$ spectrum, according to the relation

$$\left(\frac{dn_t}{dt}\right) = \sigma_p^0 \Phi N_t . \tag{2.5}$$

Let us note that, in both cases, absolute measurements of the optical cross sections are possible, provided that N_t has been measured previously, by running DLTS, for example.

Here one must comment on the influence on such measurements of the free-carrier tail in the depletion region, which has been shown to be responsible for misinterpretations of experimental results concerning some deep levels in GaAs and InP.[31,32] Taking into account this so-called "transition" region, Eq. (2.1) must be rewritten, in each point x of the depletion region, as (n-type material)

$$\frac{dn_t}{dt}(x,t) = -\sigma_n^0 \Phi n_t(x,t) + [\sigma_p^0 \Phi + C_n n(x)] p_t(x,t), \tag{2.6}$$

where C_n is the electron capture rate of the level; $n(x)$ represents the free-carrier tail in the depletion region. Equation (2.6) shows that, in the case of initial condition (i) (all centers filled with electrons), this transition region has no influence, since $p_t(x, 0) = 0$ for whatever values of x. The situation is different in the case of conditions (ii), because within the transition region, the centers cannot be filled with holes, due to the presence of the free-carrier tail [$n_t(x, 0) \neq 0$ in this region], so that some contribution of σ_n^0 might be expected in the derivative of the photocapacitance transient. In fact, such a perturbation arises only at the edge of the transition region, i.e., next to that point where the Fermi level crosses the level; deeper in the material, where $C_n n(x)$ is much larger as compared to the optical emission rates, the occupancy of the level remains unchanged under illumination. This "edge" region thus concerns only a few number of centers and its effect can be neglected as soon as a large enough (a few volts) reverse bias and not too high a photon flux are used.[30]

The proper initial conditions can be experimentally achieved through electrical excitation, using a majority-carrier pulse on (i) an n-type sample and (ii) a p-type sample. Using junctions instead of Schottky barriers, minority carriers can also be injected on minority-carrier traps through injection pulses; this leads to the $\sigma_p^0(h\nu)$ [or $\sigma_n^0(h\nu)$] spectra for hole (or electron) traps in n- (or p-) type material. Thermal excitation can also be used to reach the proper carrier populations on the traps. Temperature is then chosen such that the investigated level is completely filled with electrons or holes at thermal equilibrium. Levels in the upper half of the band gap empty at a high enough temperature, so that their $\sigma_p^0(h\nu)$ spectrum can be obtained, starting from such an initial condition. Conversely, levels in the lower half are filled with electrons at a proper temperature, and their $\sigma_n^0(h\nu)$ cross section can be directly studied. Finally, optical excitation can also be used, but only if one can find a photon excitation energy $h\nu_{ex}$ such that $\sigma_n^0(h\nu_{ex}) \gg \sigma_p^0(h\nu_{ex})$ or $\sigma_n^0(h\nu_{ex}) \ll \sigma_p^0(h\nu_{ex})$; this arises for levels located far from the middle of the band gap.

These different possible excitations lead to different DLOS modes of operation: electrical DLOS, thermal DLOS, and optical DLOS.[30,33] We have summarized for each in Table I the initial condition reached, and the optical cross section measured, depending on the type of the material and the position of the level in the band gap. It turns out that such DLOS measurements will solve the problem of measuring $\sigma_n^0(h\nu)$ and $\sigma_p^0(h\nu)$ in almost every case. One question remains: the selectivity of the method, i.e., its ability to provide the optical properties of a well identified level. It can be obtained by coupling DLOS with DLTS; this will be better demonstrated on practical examples, as done in the following.

B. Experimental setup

Indeed, the main experimental difficulty is to measure the derivative of the capacitance transient at the beginning of the illumination with sufficient accuracy. This requires (i) to send into the diode a high monochromatic photon flux in order to have a significant derivative, (ii) to measure the derivative within a small enough delay after excitation, and (iii) to use repetitive excitation-illumination cycles and a sampling-averaging technique to increase the signal-to-noise ratio. We have used an optical system which includes a prism monochromator and an infrared microscope to focus the light beam onto the diode area (Schottky barriers, 500-μm diameter, approximately). The capacitance is measured with a 200-kHz lock-in amplifier followed by either a digital voltmeter or a boxcar. The measurement cycles are programmed using an on-line calculator which controls the sample temperature, the electrical excitation pulses, the dc bias voltage applied to the barrier, the monochromator wavelength, and the light beam shutter. The calculator also collects the data, computes the derivative after proper averaging on a fixed number of cycles, and finally displays the optical cross section spectrum corrected for the photon flux variation $\Phi(h\nu)$. The diagram of this experimental setup is shown on Fig. 1. The capacitance measurement resolution lies between 10^{-4} and 10^{-5}, and the minimum time constant is about 1 ms.

Table II represents the experimental sequences corresponding to the three DLOS modes of operation: time dependence of the different excitations and of the relevant changes in capacitance. The derivatives are generally measured over a tenth of the optical transient time contant τ^0, which is a few seconds, depending on the wavelength and the level investigated. Obviously, such an experimental setup allows many other measurements, such as classical[20] (electrical) DLTS or optical DLTS at variable wavelength,[21] to be carried out

TABLE I. DLOS modes of operation. The table indicates the initial condition reached in the level and the optical cross section measured through DLOS, depending on the type of the material and the position of the level in the band gap.

	MAJORITY-CARRIER PULSE	MINORITY-CARRIER PULSE	HIGH TEMPERATURE STEADY-STATE	OPTICAL EXCITATION
Junction / Material	p-n or Schottky	p-n only	p-n or Schottky	p-n or Schottky
n type	Centers filled with electrons $\sigma_n^o(h\nu)$	(p^+-n) Centers filled with holes $\sigma_p^o(h\nu)$	Centers filled with holes $\sigma_p^o(h\nu)$ Centers filled with electrons $\sigma_n^o(h\nu)$	Centers filled with holes $\sigma_p^o(h\nu)$ Centers filled with electrons $\sigma_n^o(h\nu)$ (depends on lattice relaxation)
p type	Centers filled with holes $\sigma_p^o(h\nu)$	(n^+-p) Centers filled with electrons $\sigma_n^o(h\nu)$	Centers filled with holes $\sigma_p^o(h\nu)$ Centers filled with electrons $\sigma_n^o(h\nu)$	Centers filled with holes $\sigma_p^o(h\nu)$ Centers filled with electrons $\sigma_n^o(h\nu)$ (depends on lattice relaxation)
EXPERIMENT	ELECTRICAL D L O S		THERMAL DLOS	OPTICAL DLOS

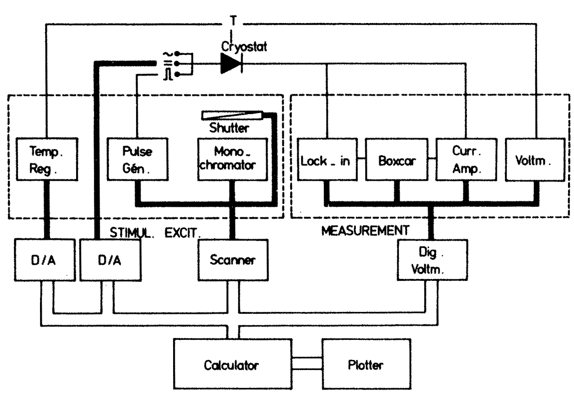

FIG. 1. Schematic drawing of the experimental setup used for deep-level optical spectroscopy (DLOS). The system allows many other experimental techniques involving junction, especially deep-level thermal spectroscopy (DLTS), to be carried out by suitable software manipulations.

by suitable software manipulations. For example, Table III shows the experimental sequences corresponding to DLTS.

The results reported below have been obtained using Au-GaAs Schottky barriers. All samples (grown in Laboratoires d'Electronique et de Physique Appliquée, Paris and Radiotechique Compelec, Caen) were n-type, in the 10^{15}–10^{16} cm^{-3} range.

C. Experimental study of the "O" level in GaAs

We have used DLOS to analyze first the deep so-called "oxygen" (Ref. 34) or $EL2$ (Ref. 35) level in GaAs. A lot of work has been recently devoted to this electron trap because of its presence in all bulk and vapor-phase epitaxial (VPE) materials[10,14,36,37] and of some particular properties[38,39] Pressure experiments,[2,40] alloying ef-

TABLE II. Experimental sequences involved in DLOS. The time dependences of the different excitations used to carry out the three DLOS modes of operation are shown. The points on the relevant capacitance changes indicate the sampling procedure leading to the DLOS signal.

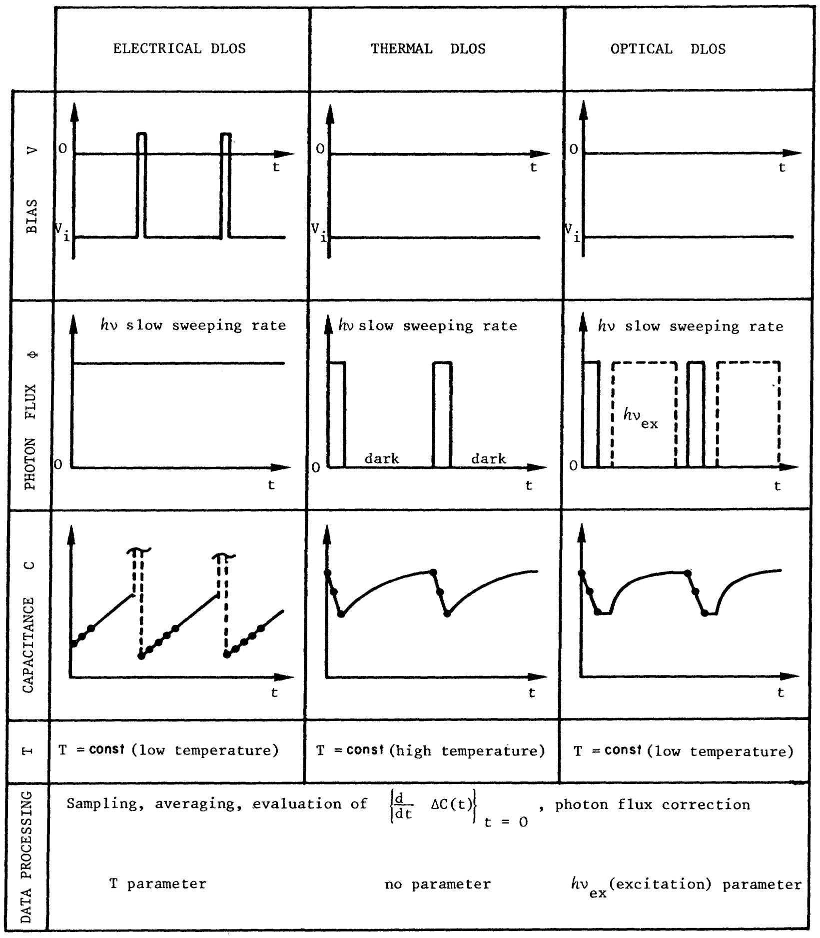

fect in $Ga_{1-x}In_xAs$,[37] electric field effects,[41] and many optical measurements[10,11,38,39,42] have been carried out on this level together with theoretical calculations.[43,44] This activity greatly justifies a careful analysis of the optical cross sections associated with this level, despite the fact that its exact microscopic origin is still unknown: In particular, it is not yet clear whether it is really related to oxygen.[45,46]

1. Measurement of $\sigma_p^0(h\nu)$

The thermal characteristics of this level have been measured by several workers;[34,47–49] they generally find a binding energy E_n around 0.75 eV for the electron trapped on the level near 300 K. Even if this value can be discussed with respect to capture cross-section temperature dependence,[34] everyone agrees with the signature of the level,[35] which corresponds to an electron thermal emission rate $e_n \sim 1\ \mathrm{min}^{-1}$ at 300 K and no hole emission ($e_p = 0$). This level thus being empty under dark equilibrium conditions around 300 K, the $\sigma_p^0(h\nu)$ cross section can be obtained through thermal DLOS, as pointed out before (cf. Table I). If temperature is chosen such that e_n is not too large as compared to the optical emission rate $\sigma_p^0\Phi$, all the measurement cycle can be performed at this fixed temperature; this greatly simplifies the experiment. Indeed, temperature cycles would have to be realized in order to get $\sigma_p^0(h\nu)$ at lower temperatures. Figure 2 shows the $\sigma_p^0(h\nu)$ spectrum as obtained at 305 K.

The main features of this experimental curve are the accuracy of the results and the very large photon energy range in which $\sigma_p^0(h\nu)$ is determined. Both could never be obtained with previously used techniques. Moreover, the method used here is truly selective, i.e., one can be sure that the whole curve shown in Fig. 4 is associated with the "O" level only. Indeed, shallower levels are com-

TABLE III. Experimental sequences involved in DLTS. The time dependences of the different excitations used to carry out classical (electrical) and optical DLTS are shown. The points on the relevant capacitance changes indicate the sampling procedure leading to the DLTS signal.

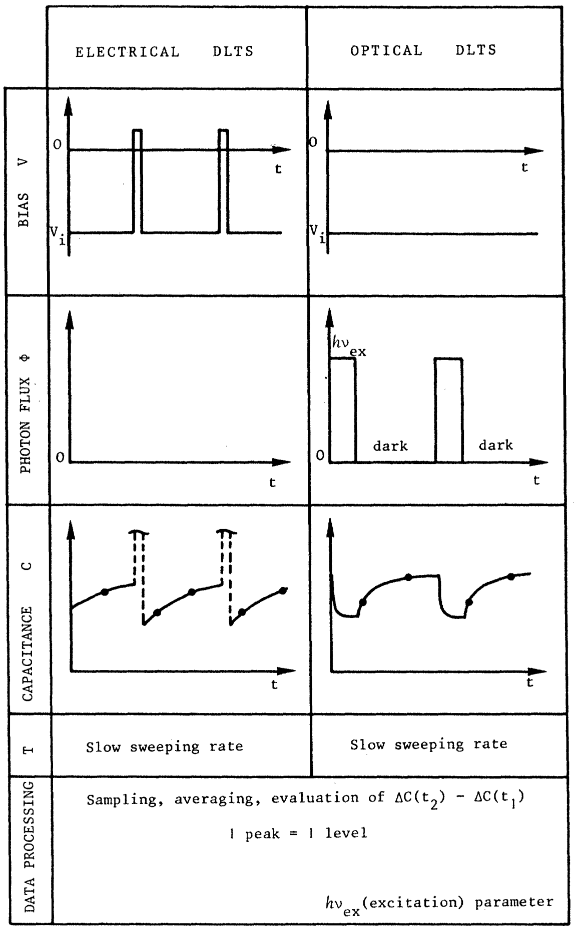

pletely ionized at 300 K and, anyway, they have high thermal emission rates and their optical responses are negligible. As for deeper centers, they do not empty in the dark at this temperature and thus do not contribute to the initial derivative of the optical transients, provided that measurement is made after some cycles at each photon energy, so that optical equilibrium in the level is reached. This assertion can easily be verified, analyzing the thermal transients following the end of the illumination periods: If several levels were simultaneously involved, these transients would show several exponential parts. A simple way to do this is to run optical DLTS spectra at various photon energies. One is shown on Fig. 3 for $h\nu_{ex} = 1.30$ eV. It can be seen that at 305 K, only the "O" level is involved. The same result has been obtained

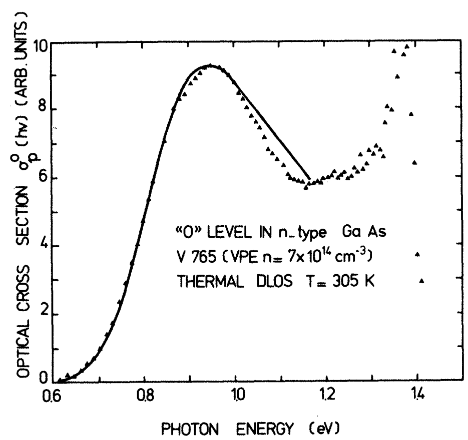

FIG. 2. Spectral distribution of the optical cross section $\sigma_p^0(h\nu)$ for the "oxygen" level in GaAs, as directly obtained through a 15-min thermal DLOS scan at 305 K (▲). The solid line represents the calculated curve using Eq. (4.11) with $E_p = 0.69$ eV, $d_{FC} = 0.12$ eV ($\Theta \simeq 2\times 10^{-2}$), and $\alpha^{-1} \simeq 5$ Å ($m_p = 0.35$) (see Sec. IV).

throughout the photon energy range.

The $\sigma_p^0(h\nu)$ curve shows a rather sharp peak around 0.95 eV, followed by an increase above 1.15 eV. Their physical meaning will be discussed in Sec. IV. The signal drop above 1.35 eV is likely to be due to intrinsic absorption (indeed, the Schottky barrier is illuminated through the bulk).

2. *Measurement of $\sigma_n^0(h\nu)$*

With an n-type Schottky barrier, $\sigma_n^0(h\nu)$ can be obtained using electrical DLOS (cf. Table I). As electrical excitation is now used, the experiment can be performed at different temperatures, which was not possible in the preceding case. Figure 4 shows the $\sigma_n^0(h\nu)$ spectra obtained between 85 and

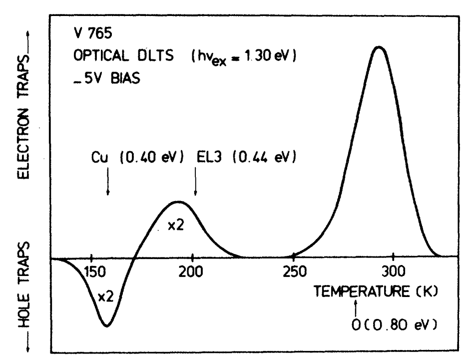

FIG. 3. Optical DLTS spectrum obtained on sample V765, using a 1.30-eV excitation beam. A set of such spectra, recorded at variable wavelengths, allows one to be sure that only the "O" level in involved in the thermal DLOS curve ($T = 305$ K) shown in Fig. 2.

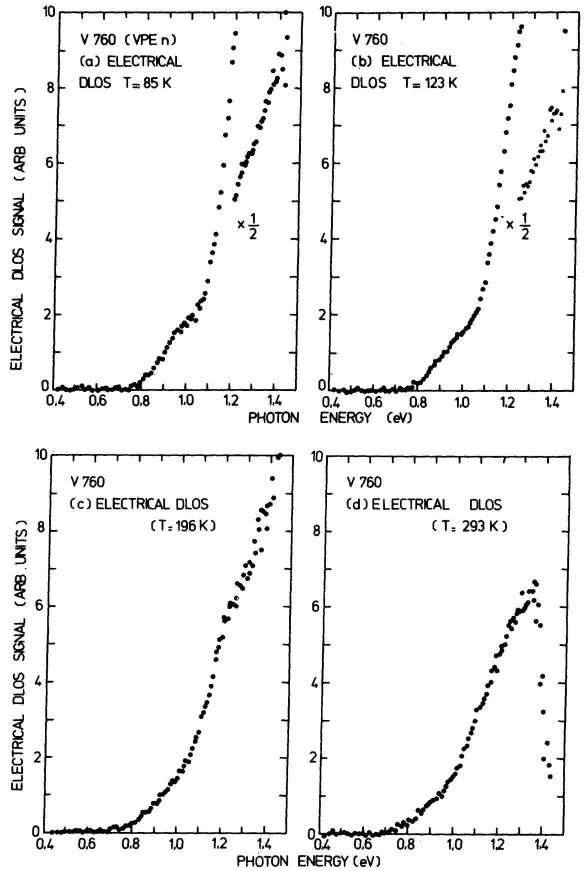

FIG. 4. Typical example of the temperature dependence of electrical DLOS spectra obtained on samples containing more than one deep level. The large signal drop above 1.1 eV between $T=123$ and 196 K is due to the thermal ionization of the copper-related hole trap between these two temperatures (See Fig. 5).

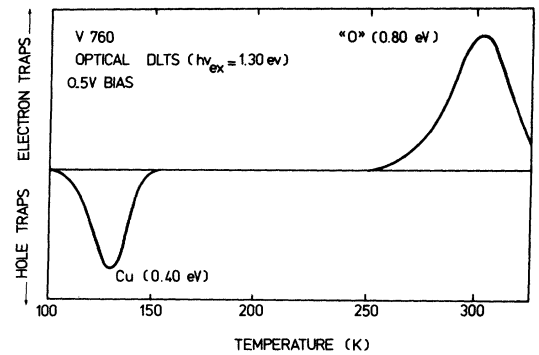

FIG. 5. Optical DLTS spectrum obtained on sample V760, using a 1.30-eV excitation beam. This figure shows that the electrical DLOS spectra recorded below 150 K [Figs 4(a) and 4(b)] represent the sum of the $\sigma_n^0(h\nu)$ contributions of copper and "O" levels, whereas above 150 K [Figs. 4(c) and 4(d)], only the latter is involved.

293 K in another sample containing the "O" level. Four transition thresholds can be seen around 0.80, 1.05, 1.25, and 1.40 eV on the low-temperature curve.

Now, a question arises: Is the procedure selective, i.e., is it possible to associate the whole spectra to the "oxygen" level? Of course, the answer is negative, because at low temperatures, all deep levels being filled with electrons at the end of the electrical excitation pulses, the initial derivative of the capacitance transients is related to the sum of the contributions of all the levels, i.e., to

$$\sum_i N_{t_i}\sigma^0_{n_i}(h\nu)\Phi(h\nu)\,.$$

However, optical DLTS can be used again to clarify the situation. Figure 5 shows the optical DLTS spectrum obtained with $h\nu_{ex}=1.30$ eV, i.e., in the part of the DLOS spectrum where all the levels can be expected to contribute. Indeed, it turns out that besides the "O" level, another trap is optically excited at this photon energy: It is a hole trap. Classical DLTS analysis of this hole trap with different gate delays yields an activation energy of about 0.40 eV and a signature very close to copper.[34,50] This is not surprising, since this level is commonly found in VPE layers.[10,14,36,37] One can thus assert that the DLOS spectra recorded below 150 K [Figs. 4(a) and 4(b)] represent the sum of the $\sigma_n^0(h\nu)$ cross sections associated with "O" and copper levels. But above 150 K, the thermal hole-emission rate of the copper level is very large as compared to optical rates, so that its optical response vanishes, and the whole DLOS curve is now related to the "O" level only. This applies for the 196-K [Fig. 4(c)] and 293-K [Fig. 4(d)] curves. The 196-K curve still clearly shows thresholds at 0.80, 1.05, and 1.25 eV, so one can be sure that they are all associated with the "O" level. We have checked that these transitions systematically appear in electrical DLOS spectra in the presence of this level. The main change in the DLOS curve between 123 and 196 K, which are on both sides of the copper DLTS peak, lies in the amplitude of the bands 1.25 and 1.40 eV (Fig. 5). Both are much reduced between these two temperatures, which means that copper brings a contribution above about 1.1 eV to the low-temperatures DLOS spectra. This point will be better demonstrated in Sec. IID.

This discussion shows how DLOS and optical DLTS can be coupled to get the spectral response of each deep level. Indeed in this case, the selectivity is not perfect, since at low temperatures, one cannot separate the contributions of the different levels. Figure 6 gives another example.

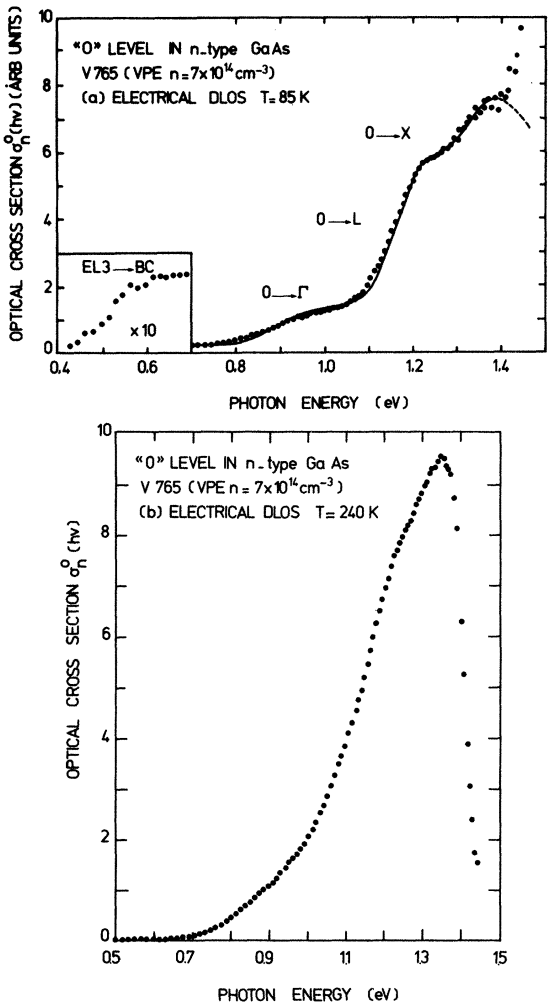

FIG. 6. Spectral distribution of the optical cross section $\sigma_n^0(h\nu)$ for the "oxygen" level in GaAs, as obtained by electrical DLOS at 85 K (a) and 240 K (b) (sample $V765$). The lower energy band in the $T = 85$ K spectrum does not appear at 240 K, and can thus unambiguously be attributed to level $EL3$ (See Fig. 3). The solid line [Fig. 6(a)] represents the calculated curve using Eq. (4.11) with $P_L = 0.25$, $P_X = 0.1$, the other parameters being taken from the previous $\sigma_p^0(h\nu)$ adjustment (See Sec. IV).

In this sample, corresponding to the optical DLTS spectrum shown in Fig. 3, the concentration of copper is less than in the preceding one, but another small electron trap can be seen. The DLTS analysis locates this level at 0.44 eV below the conduction band, close to the signature of $EL3$.[35] Figure 6 shows the corresponding electrical DLOS curves. At 85 K [Fig. 6(a)], besides the 0.80, 1.05, 1.25, and 1.40 eV thresholds, another optical response is observed, with a threshold at about 0.45 eV. This response disappears above 240 K [Fig. 6(b)], in agreement with the optical DLTS spectrum. The 0.45-eV threshold band can thus unambiguously be attributed to the 0.44-eV electron trap. The other difference with the low temperature DLOS curve of Fig. 4 is the reduced amplitude of the 1.05-eV and 1.25-eV threshold bands, as expected from the lower copper concentration in the material. Indeed, comparison between Figs. 4(c) and 6(a) suggests that copper contribution can be neglected in the latter. As a consequence, above 0.80 eV, the Fig. 6(a) spectrum represents the "O" level $\sigma_n^0(h\nu)$ photoionization cross section at 85 K. The structure which can be seen on this curve suggests that transitions to the various valleys of the conduction band (Γ, L, X) are involved, as will be discussed in Sec. IV.

D. Copper-related hole trap in GaAs

1. *Measurement of* $\sigma_n^0(h\nu)$

In VPE material, the copper spectrum is always mixed with the "O" spectrum, as discussed above. As the Cu DLTS peak appears at lower temperature than the "O" one, its optical contributions cannot be simply isolated by a good temperature choice. Indeed the $\sigma_n^0(h\nu)$ curve could be obtained by the difference between two electrical DLOS spectra, run at temperatures chosen on both sides of the Cu DLTS peak: $T = 123$ and 196 K, for instance [Figs. 4(b), 4(c), and 5]. However, this method is not very precise, because the "oxygen" spectrum slightly changes between the two temperatures.

We prefer to take advantage of a very interesting property of the "O" level. Using an intense illumination around 1.1 eV, it is possible to quench its optical response.[38,39] Afterwards, everything appears as if the "O" level were not present in the material, as long as an electrical injection pulse is not sent into the diode. Of course, this last observation implies that electrical DLOS cannot be used, but optical DLOS does apply for such a trap (Table I): 0.50-eV illumination periods are used to refill the level with electrons at each cycle [this energy is indeed well below the threshold of the Cu→conduction band (CB) transition]. Figure 7 shows the $\sigma_n^0(h\nu)$ curve as obtained through this method at $T = 85$ K. The threshold of the transitions is about 1.1 eV, in agreement with above conclusions. Indeed, this energy is very close to the 1.05-eV threshold band observed on the "O" level $\sigma_n^0(h\nu)$ curve; this explains why the latter has been commonly attributed to copper.[10,37] DLOS coupled to DLTS allows a clear identification of these two transitions.

2. *Measurement of* $\sigma_p^0(h\nu)$

Measurement of the $\sigma_p^0(h\nu)$ cross section associated with hole traps in n-type Schottky barriers is

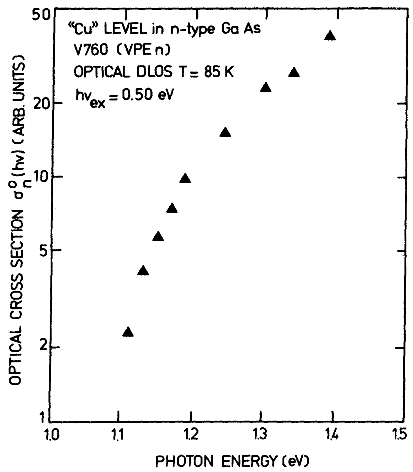

FIG. 7. Spectral distribution of the optical cross section $\sigma_n^0(h\nu)$ for the copper-related hole trap in GaAs, as obtained through an optical DLOS scan at 85 K, with 0.50-eV illumination periods. The "O" level optical response has been previously quenched by a 1.1-eV intense illumination.

only possible through optical DLOS. In the present case, the level cannot be refilled with holes using optical excitation. However, optical DLOS allows $\sigma_p^0(h\nu)$ to be obtained rigorously up to the Cu–CB threshold energy. Indeed, whatever the level occupancy at the end of the excitation period, the initial derivative of the following capacitance transient is proportional to $\sigma_p^0(h\nu)$ as long as $\sigma_n^0(h\nu)$ is zero, i.e., up to 1.10 eV here. Figure 8 shows the $\sigma_p^0(h\nu)$ curve thus obtained at $T = 85$ K with a 1.40-eV excitation light beam. The threshold en-

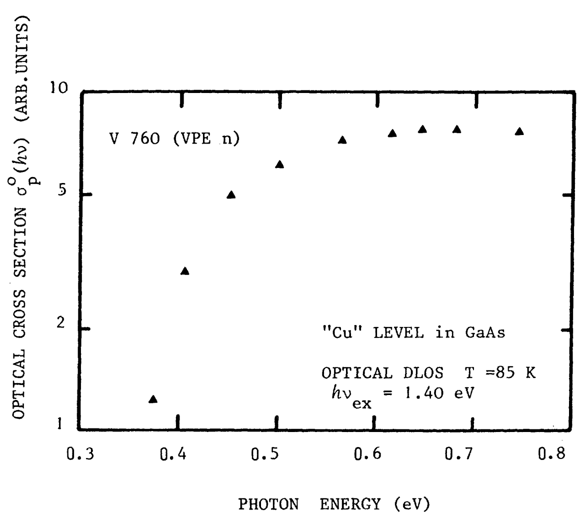

FIG. 8. Spectral distribution of the optical cross section $\sigma_p^0(h\nu)$ for the copper-related hole trap in GaAs. This curve was obtained through optical DLOS at 85 K, using 1.40-eV excitation beam.

ergies of $\sigma_n^0(h\nu)$ and $\sigma_p^0(h\nu)$ suggest that lattice relaxation is very weak for this level, in agreement with the hole-capture cross-section temperature dependence.[34] This example shows that optical DLOS is well suited to levels located far from the middle of the band gap. Both $\sigma_n^0(h\nu)$ and $\sigma_p^0(h\nu)$ cross sections can indeed be obtained at low temperature.

E. Chromium in GaAs

Depending on the position of the Fermi level in the band gap, several levels have been observed in chromium-doped semi-insulating or conducting materials.[3-7,15,17,51-53] For the capacitance measurements described here, conducting samples are indeed required, so we have used an n-type sample. In such material, a level is known to lie near the middle of the band gap.[34,54,55] DLTS yields an activation energy of 0.76 eV for thermal transient time constant, corresponding to a signature very close to $EL1$ in Martin's classification.[35] The DLTS peak of this level is generally overlapping with the "oxygen" one, so that the contributions of these two levels to DLOS spectra cannot be separated through measurements at different temperatures. However, the investigated material did not contain the "oxygen" level; this could be easily checked by the lack of the photocapacitance quenching effect which is characteristic of this level. No other electron or hole trap could be seen on optical DLTS spectra.

In such a material containing a unique level, the $\sigma_n^0(h\nu)$ spectrum can be obtained at various temperatures using electrical DLOS. The result of this analysis is shown on Fig. 9. The main feature of the curves is the sharp peak around 0.9 eV, which has been tentatively attributed to internal transitions between two localized states of the same center (the excited one being resonant in, or near, the conduction band[3]). So far as no other levels are present in the material, the increase observed above 1 eV in the DLOS signal must also be assigned to transitions from $EL1$ to the conduction band.

Measurement of $\sigma_p^0(h\nu)$ for the same level is very difficult. Indeed, thermal DLOS cannot be used as in the case of "O", because the two thermal emission rates e_n and e_p have the same order of magnitude at high temperature.[34] Therefore, in the high-temperature limit, the centers are not completely filled with holes in the reverse-biased diode. This is clearly demonstrated by the increase in capacitance observed under illumination at 0.9 eV after thermal equilibrium in the level.[30] Optical DLOS also cannot be used in a simple way, because the thresholds of the $\sigma_n^0(h\nu)$ and $\sigma_p^0(h\nu)$ spectra are likely to lie very close to each other.

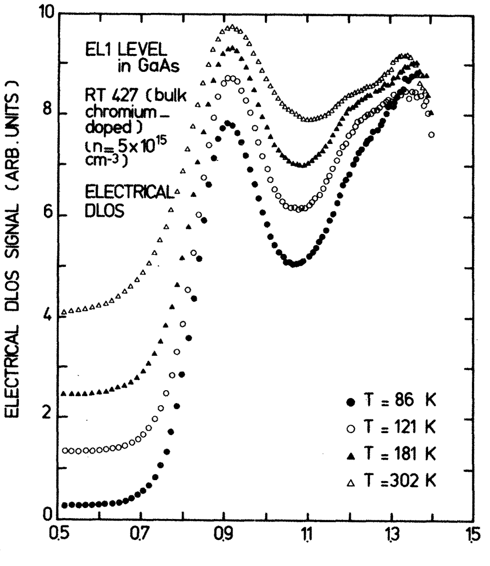

FIG. 9. Example of the temperature dependence of electrical DLOS spectra in the presence of a single deep level: *EL*1 in GaAs. The four superimposed curves, representing the optical cross-section spectra for the transitions between the level and the conduction band, show temperature broadening due to phonon coupling.

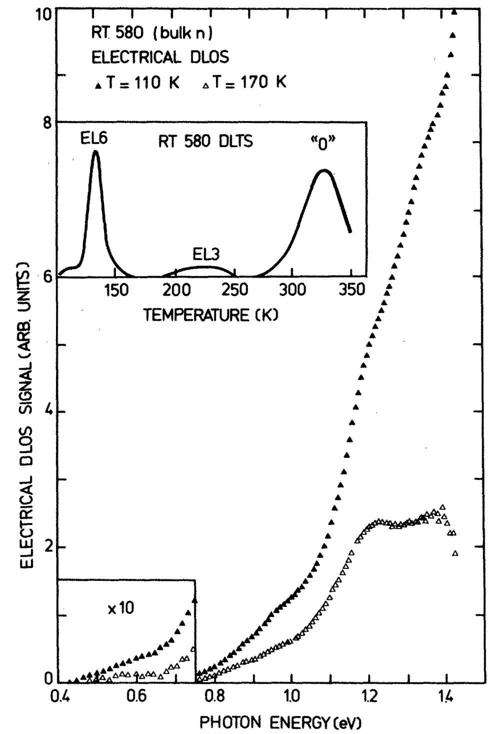

FIG. 10. An illustration of DLOS-DLTS coupling: *EL*6 in bulk GaAs. The figure shows two electrical DLOS curves recorded at temperatures chosen on both sides of *EL*6 DLTS peak (see the DLTS spectrum in the insert). The signal drop between 110 and 170 K gives the optical response of *EL*6 alone. Note the lack of a large signal below 0.80 eV on the low-temperature curve.

It is thus impossible to experimentally achieve an initial condition where all the traps are filled with holes in an n-type sample. Let us note that such a situation is a very uncommon one, probably unique in GaAs. However, it must be pointed out that $\sigma_p^0(h\nu)$ would be directly obtained, running electrical DLOS on a p-type sample.

F. Main electron trap in bulk GaAs

Apart from the "oxygen"- and copper-related levels discussed previously, another shallower electron trap is commonly observed in bulk GaAs. DLOS allowed us to discover its particular optical behavior.

This trap appears near 150 K in a bulk sample DLTS spectrum, as shown in the inset of Fig. 10. DLTS yields a 0.31-eV activation energy for electron emission and a signature very close to *EL*6 in Martin's classification.[35] The concentration of this level nearly equals that of "O", which appears above 300 K on the same spectrum. Two other electron traps can be observed in a much lower concentration, near 220 K (*EL*3) and 290 K (low-temperature enlargement of the "O"-related DLTS peak). No hole trap could be detected through optical DLTS ($h\nu_{ex}$ = 1.25 eV).

Figure 10 shows the electrical DLOS spectrum recorded at T = 110 K, a temperature where all the levels give their contribution. No important signal can be seen in the region where *EL*6 should respond, i.e., below the "O" → CB transition threshold. Only a weak band is detected, with a 0.45-eV threshold energy, close to the *EL*3 → CB one (See Fig. 6). Moreover, no additional band appears above 0.80 eV, where the previously identified thresholds are observed; only the increased importance of the 1.25-eV threshold energy band (compare with Fig. 6) must be noted.

In order to identify the real $\sigma_n^0(h\nu)$ contribution of *EL*6, we have run electrical DLOS at T = 170 K, i.e., on the other side of its DLTS peak; the result is shown on Fig. 10. The most striking feature is the almost 50% reduced amplitude of the signal between 0.75 and 1.15 eV; this means that the $\sigma_n^0(h\nu)$ cross sections associated with "O" and *EL*6 are very similar in this photon energy range. Also observed between these two temperatures are the reduced amplitudes of the low-energy band—which means that it is partly related to *EL*6—and of the high-energy one. The 0.45-eV threshold band seen on the T = 170 K curve must be related to *EL*3, which is not yet thermally ionized at this temperature.

Figure 11 shows the $\sigma_n^0(h\nu)$ spectrum obtained from the difference between the two DLOS curves of Fig. 10. This spectrum might eventually contain a contribution of a hole trap appearing in the same temperature range as $EL6$, copper for example, which thus would not be eliminated with this method. We have in vain looked for the characteristic optical refilling of copper from the valence band at low temperature, concluding that it is absent in the material. As a consequence, Fig. 11 represents the $\sigma_n^0(h\nu)$ cross section associated with $EL6$ near $T = 110$ K, with a small possible error due to the change of the "oxygen" $\sigma_n^0(h\nu)$ curve between 110 K and 170 K. This $\sigma_n^0(h\nu)$ spectrum is very similar to the "O" level one: The 0.80- and 1.05-eV threshold bands are found with the same ratio, the 1.25-eV one being more important. A fourth band is observed at lower energy with a very weak intensity.

In order to complete this information, we investigated the optical transitions involving the valence band, using thermal DLOS at $T = 115$ K. Surprisingly, we found no trace of such transitions, i.e., $\sigma_p^0(h\nu)$ appears to be null all over the photon energy range. All these observations suggest a large lattice relaxation effect for this level, as will be discussed in detail in Sec. IV.

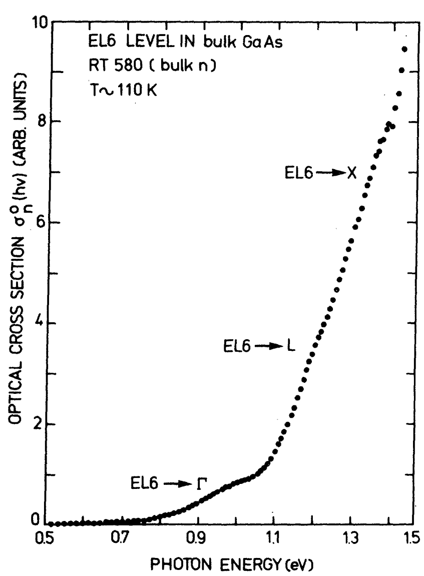

FIG. 11. Spectral distribution of the optical cross section $\sigma_n^0(h\nu)$ for $EL6$ in bulk GaAs, as obtained from the difference between the two DLOS curves of Fig. 10. The large difference between thermal (~0.30 eV) and optical (~0.8 eV) ionization energies suggests strong lattice relaxation effects for this level. The direct coupling of DLOS with DLTS allows an unambiguous detection of such phenomena.

G. Radiation-damage levels in GaAs

Most of the deep traps in GaAs, especially those which are characteristic of a particular growth technique [A and B levels in Liquid-phase epitaxial (LPE) material,[20] $EL2$ in VPE layers (Sec. II C), $EL6$ in bulk GaAs (Sec. II F)] still have unknown microscopic origins. Identification of some of them to lattice defects is one of the aims of radiation-damage levels investigations in this material.[56] We have been mainly interested here in an electron trap ($E3$), created by electron and proton irradiation at 300 K (Refs. 56 and 57) and 77 K (Ref. 58) in VPE material, which has been tentatively attributed to a gallium vacancy V_{Ga} (Ref. 59) or to an antisite defect As_{Ga} (Ref. 60).

The DLTS spectrum of an n-type VPE sample, irradiated with electrons at room temperature, is shown in the inset of Fig. 12. Three electron traps are seen, which can be identified to $E3$, $E4$, and $E5$ from Lang's analysis.[61] A thermal activation energy of 0.31 eV is found for electron emission from $E3$ into the conduction band, in agreement with Pons's determination on equivalent samples.[62] Lang has recently proposed a very large

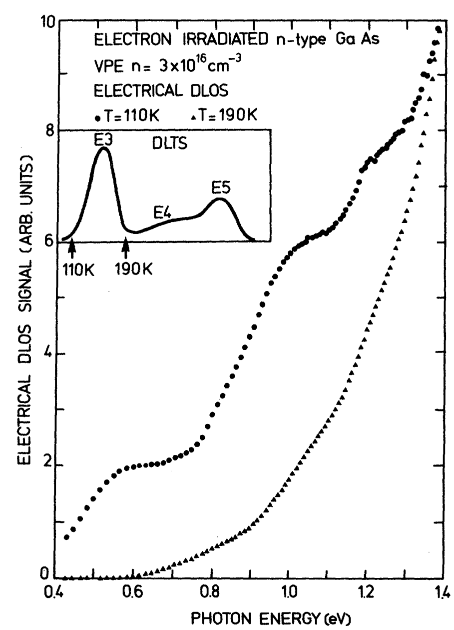

FIG. 12. Another example of selectivity with DLOS: $E3$ radiation-damage level in GaAs. Three bands can be seen on the low-temperature (110 K) electrical DLOS curve of an electron-irradiated sample, which might be tentatively attributed to the three $E3$, $E4$, and $E5$ created levels (see the DLTS spectrum in the insert). However, the same DLOS curve recorded at 190 K, i.e., a temperature where $E3$ is thermally ionized, shows that this level is actually involved over the whole low-temperature curve.

lattice relaxation effect for $E3$,[59] which would explain its large hole-capture cross section (σ_p ~50 Å^2). This hypothesis can be easily checked by an analysis of the $\sigma_n^0(h\nu)$ cross section associated with this level. Of course, $E3$ cannot be isolated in a material, since all the defects are created simultaneously and anneal during the same stage.[56] And again, DLOS appears as the unique technique enabling such an analysis.

Figure 12 shows the electrical DLOS spectra recorded at $T = 110$ and 190 K, i.e., on both sides of $E3$ DLTS peak; the difference between the two curves is shown in Fig. 13. Let us note that one of the radiation-induced hole traps ($H1$) also appears between 110 and 190 K in a DLTS spectrum[61]; it must be responsible for the bump seen near 1.2 eV in Fig. 13, as expected from its hole-emission–thermal-activation energy ~ 0.25 eV.[61] Below 1.1 eV, Fig. 13 thus represents the $\sigma_n^0(h\nu)$ optical cross section associated with $E3$. The main features of this experimental curve are again the observed structure related to the CB density of states and the threshold energy, which implies only weak lattice relaxation. It would be interesting to check this last point by analyzing the $\sigma_p^0(h\nu)$ spectrum associated with the same level. This curve will be obtained through thermal DLOS near $T = 130$ K or optical DLOS with a 0.60-eV excitation beam. Finally, let us note that the high-temperature spectrum on Fig. 12 represents the sum of the $\sigma_n^0(h\nu)$ contributions of the other radiation-induced levels.

III. COMPARISON OF DLOS WITH OTHER EXPERIMENTAL RESULTS

In order to demonstrate the validity of DLOS, we shall now give a comparison between our results and those obtained through other experimental techniques, either carried out in our laboratory or reported in the literature. As the "oxygen" level has been the most commonly investigated, this discussion will be focused on this center.

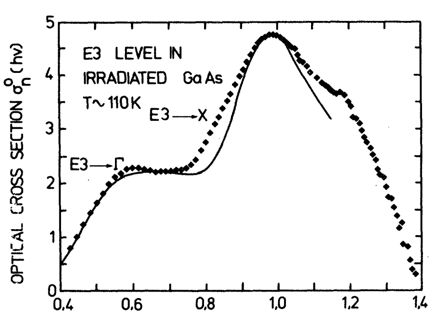

FIG. 13. Spectral distribution of the optical cross section $\sigma_n^0(h\nu)$ for $E3$ in irradiated GaAs, as obtained from the difference between the two DLOS curves of Fig. 12. The solid line represents the calculated curve using Eq. (4.11) with $E_n^0 = 0.44$ eV, $d_{FC} = 0.2$ eV ($\Theta \simeq 4\times 10^{-2}$), $\alpha^{-1} = 8$ Å ($m_n = 2$), $P_L = 0$, and $P_X = 0.15$.

A. Complete analysis of photocapacitance transients

If a temperature is chosen such that the thermal emission rate e_n and the optical ones $\sigma_n^0(h\nu)\Phi(h\nu)$ and $\sigma_p^0(h\nu)\Phi(h\nu)$ have the same order of magnitude, both thermally and optically induced photocapacitance transients can be recorded, giving two time constants: $\tau = e_n^{-1}$ ($e_n \gg e_p$) in the dark, and $\tau^0(h\nu) = [e_n + \sigma_n^0(h\nu)\Phi(h\nu) + \sigma_p^0(h\nu)\Phi(h\nu)]^{-1}$ under illumination. Two amplitudes, related to the trap concentration N_t (in the dark) and the ratio

$$N_t[e_n + \sigma_n^0(h\nu)\Phi(h\nu)][e_n + \sigma_n^0(h\nu)\Phi(h\nu) + \sigma_p^0(h\nu)\Phi(h\nu)]^{-1}$$

(under illumination), can also be extracted from these transients. From these four quantities, both σ_n^0 and σ_p^0 cross sections can be obtained at each photon energy. Indeed, it is a tedious and time-consuming work, which only applies in a narrow temperature range.

We have made such an analysis for the "O" level, which is a very difficult case because the level lies in the middle of the band gap, i.e., with a maximum overlap between $\sigma_n^0(h\nu)$ and $\sigma_p^0(h\nu)$. We used for this purpose one of the DLOS-investigated samples (see Fig. 3). The results, shown in Fig. 14, are much more scattered than the DLOS ones; this uncertainty is probably due to the imperfect reproducibility between each transient and to the time constant calculation. Nevertheless, the general agreement is good. In particular, the two first bands on the $\sigma_n^0(h\nu)$ curve clearly appear in Fig. 14. This confirms our earlier statement that both are associated with the "O" level. Indeed, it should be emphasized that this very elementary technique is quite selective: The sum of the refilling and emptying transient amplitudes at each photon energy, equal to the thermal transient amplitude, allows one to be sure that no other level is involved.

B. High-temperature steady-state photocapacitance

We have shown previously that low-temperature steady-state photocapacitance cannot be used to determine the deep-level optical cross sections (Sec. II A). On the other hand, high-temperature photocapacitance can be used to a certain extent. When the thermal emission rate e_n of a level is large compared to the optical rates, the steady-state population on the level under illumination can be written as

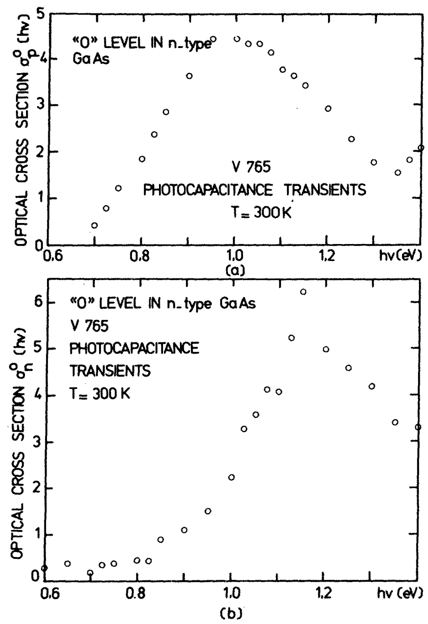

FIG. 14. Comparison DLOS–photocapacitance: $\sigma_n^0(h\nu)$ and $\sigma_p^0(h\nu)$ spectra for the "oxygen" level in GaAs, as extracted from the complete analysis of photocapacitance transients. Although much more scattered, the results of this tedious measurement are in a good agreement with our DLOS spectra (see Figs. 2 and 6).

$$(n_t)_\infty \approx N_t \frac{\sigma_p^0 \Phi}{e_n}. \tag{3.1}$$

Under such conditions, the high-temperature steady-state photocapacitance directly provides the spectral shape of the $\sigma_p^0(h\nu)$ cross section, after correction for the photon flux variation. This method applies for the determination of the optical cross section for minority-carrier emission from any trap at high temperature. Figure 15 shows the result of such an experiment run at 340 K in the "oxygen" level. Again, very good agreement is found between this curve and the DLOS measurements at room temperature (see Fig. 2). The small discrepancies are likely to be due to the temperature difference, as well as to the approximation implied in Eq. (3.1).

C. Double source differentiated photocapacitance

In this experiment as in the preceding one, a steady population of electrons and holes is created on the level investigated, but a high intensity light beam ("priming" radiation, typically 1.3 eV for GaAs) is used instead of temperature.[17] This allows the experiment to be run at low temperature. However, the capability of determining one cross section alone is lost: Both σ_n^0 and σ_p^0 are generally mixed.

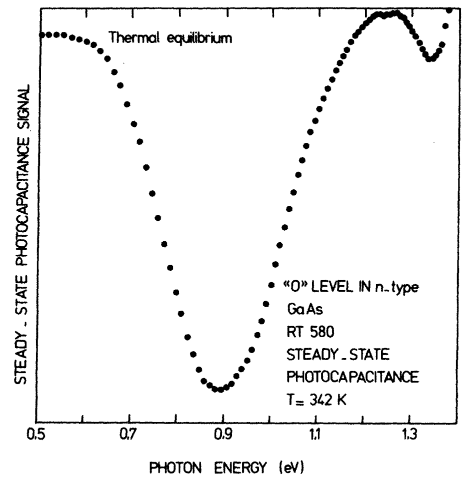

FIG. 15. Comparison DLOS–high-temperature steady-state photocapacitance. This figure shows the high temperature photocapacitance signal associated with the "O" level, which provides its $\sigma_p^0(h\nu)$ cross section spectrum. Again, good agreement is found with our thermal DLOS result (Fig. 2).

It can be easily seen that the steady-state occupancy change $(\Delta n_t)_\infty$ when the "probe" light is added to the "priming" light is given by

$$(\Delta n_t)_\infty(h\nu) = N_t[A\sigma_n^0(h\nu) - B\sigma_p^0(h\nu)]\Phi(h\nu). \tag{3.2}$$

A and B represent the initial conditions, i.e., the steady-state population on the level under priming light,

$$A = \frac{\Sigma_p^0}{\Sigma_n^0 + \Sigma_p^0} \quad B = \frac{\Sigma_n^0}{\Sigma_n^0 + \Sigma_p^0},$$

Σ_n^0 and Σ_p^0 being the priming optical rates. Moreover, in order to improve the resolution of the method, White[17] proposed to record the derivative of $(\Delta n_t)_\infty(h\nu)$ as $h\nu$ is swept at a constant rate; thus the DSDP signal is proportional to

$$\frac{d}{dh\nu}(\Delta n_t)_\infty(h\nu) = N_t\left(A\frac{d}{dh\nu}\sigma_n^0(h\nu)\Phi(h\nu) - B\frac{d}{dh\nu}\sigma_p^0(h\nu)\Phi(h\nu)\right). \tag{3.3}$$

This is a rather complex expression from which $\sigma_n^0(h\nu)$ and $\sigma_p^0(h\nu)$ cannot be extracted.

Still, in order to show that all the measurements are in good agreement, we have used the $\sigma_n^0(h\nu)$ and $\sigma_p^0(h\nu)$ curves given by DLOS (Figs. 2 and 6) to anticipate the DSDP spectrum related to the "O" level. The result of this simulation is compared in Fig. 16 to the DSDP spectrum reported by White, and attributed to the "oxygen" level.[17] The agreement is quite striking; especially, the two predicted bumps near 0.75 and 1 eV,

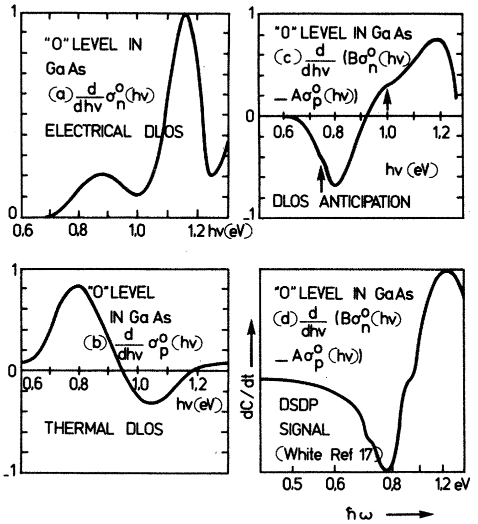

FIG. 16. Another demonstration of the validity of the DLOS results. Curve (c) shows the DSDP signal associated with the "O" level, as anticipated from our DLOS $\sigma_n^0(h\nu)$ (a) and $\sigma_p^0(h\nu)$ (b) results. The agreement with the experimental DSDP spectrum [curve (d)] reported by White (Ref. 17) is quite striking.

associated with the two first bands in the $\sigma_n^0(h\nu)$ spectrum, can be clearly seen on the experimental DSDP curve. The consistency of this analysis confirms the validity of our DLOS measurements and shows that one must be very careful when interpreting DSDP spectra as soon as deep levels are concerned.

D. Extrinsic optical absorption

Despite its poor sensitivity and nonselectivity, as pointed out previously, optical absorption is a very reliable method, involving only very simple effects. Thus we have used one of the bulk samples previously studied in our earlier optical absorption work[3,63] and performed both DLTS and electrical DLOS on it. We have reported in Fig. 17 the absorption spectrum recorded at $T = 4$ K of this n-type sample, thus corresponding to transitions to CB (Ref. 63) and the electrical DLOS curve obtained at $T = 81$ K. Again, the agreement is excellent if the temperature difference is taken into account: Owing to phonon coupling, the DLOS curve is enlarged. At the time the absorption measurements were performed, no identification of the levels was possible, and the observed structure on the spectra had been attributed to three different levels. DLTS indicates that only "oxygen" and $EL6$ are present in a large concentration in the material, both giving an optical response in each of these bands, as shown above (Figs. 6 and 11).

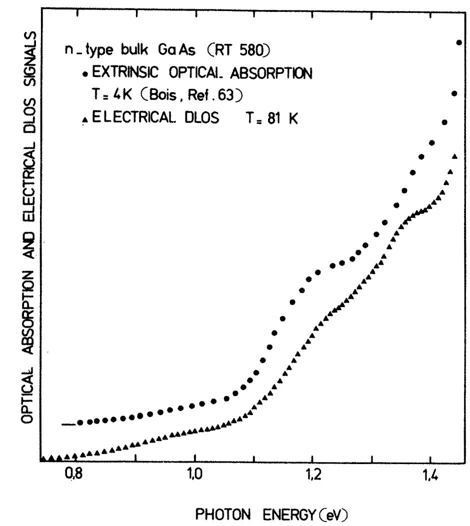

FIG. 17. Comparison between extrinsic optical absorption ($T = 4$ K) and electrical DLOS ($T = 81$ K) investigations of an n-type bulk GaAs sample. The agreement between the two curves is excellent. However, the DLOS-DLTS coupling allows an unambiguous interpretation of the observed bands in terms of GaAs-CB density-of-states distribution, rejecting the previous optical absorption conclusions of a multilevel effect.

E. Photoconductivity

As pointed out by Grimmeiss,[10] one must be very careful when interpreting photoconductivity results. Indeed, the photocurrent is a complex function of optical emission rates and capture rates; moreover, in the case of very deep levels, two-step excitations must be taken into account. Grimmeiss[10] proposed to run photoconductivity spectra at a constant photocurrent by monitoring the photon flux $\Phi(h\nu)$. This is a very nice improvement, since it ensures that the trap occupancy is constant along the whole spectrum.

Figure 18 shows the photoconductivity spectra obtained on oxygen-doped GaAs by Lin[64] (bulk, $T = 213$ K), Mircea[37] (VPE, $T = 110$ K) and Grimmeiss[10] ($T = 100$ K). All are attributed to transitions to the conduction band and must then be compared to our $\sigma_n^0(h\nu)$ spectrum given by electrical DLOS (bulk, $T = 81$ K). All the curves clearly show the 0.80- and 1.05-eV thresholds. However, photoconductivity measurements alone do not allow any interpretation of this feature, since one cannot assert (i) what deep levels are involved and (ii) whether one or several deep levels are involved in each part of the spectrum. Generally, the 1.05-eV bump was attributed to copper contamination in the sample. We have shown in Sec. II that this interpretation cannot apply to our DLOS spectrum. However, it might explain why Grim-

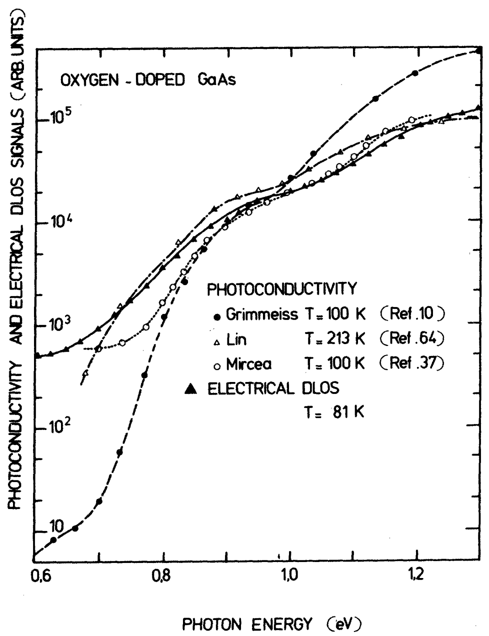

FIG. 18. As a comparison between DLOS and photoconductivity measurements, this figure shows three photoconductivity spectra obtained on oxygen-doped GaAs by Lin (Ref. 64), Mircea (Ref. 37) and Grimmeiss (Ref. 10), together with our electrical DLOS curve. All four curves clearly show the 0.80-eV and 1.05-eV threshold bands, respectively, related to the "O" → CB (Γ) and "O" → CB (*L*) transitions. Indeed, the DLOS-DLTS coupling rejects the common attribution of the latter to copper contamination.

meiss's curve presents a higher photoconductivity response above 1 eV than the others. Another feature of this last curve is its very large current range: five decades instead of two for the other experiments, because of a residual signal below the "O" level first threshold. If this background were subtracted, the agreement would probably be better.

Recently, other photoconductivity measurements of the $\sigma_n^0(h\nu)$ cross section associated with "O" at various temperatures have been reported by Tyler in high resistivity materials.[11] The results greatly differ from the preceding ones. Looking carefully at this experiment, one can find two reasons explaining this discrepancy: (i) at low temperature in high-resistivity GaAs, the quenching effect, as described by Lin[64] and us,[38,39] takes place and drastically modifies the recorded spectrum above 1 eV; (ii) the very surprising change of the spectrum shape as the temperature is increased is probably due to a change in the Fermi-level position, so that one does not measure the same optical cross section at all temperatures. This last point reflects the usual fact that photoconductivity generally mixes the $\sigma_n^0(h\nu)$ and $\sigma_p^0(h\nu)$ cross sections for a very deep level.

IV. THEORETICAL DISCUSSION

Implementation of DLOS allowed us to measure the spectral distribution of the optical cross sections associated with the main deep levels in GaAs. The main interest of such investigations is to deduce physical informations concerning the related defects. Such informations can only be obtained from a comparison between experimental results and theoretical models.

A. Optical cross sections

In the presence of an electron-phonon interaction, it is a standard approximation to write the cross section $\sigma^0(h\nu)$ as an electronic transition probality $\sigma^{el}(h\nu)$, repeated and weighted by a line-shape function given by the vibrational overlap integral.[44] The electronic matrix element for the transition between a trap t and a band b can be expressed as

$$\sigma^{el}(h\nu) \propto \frac{1}{h\nu} |\langle b, \vec{k} | -i\hbar\vec{\nabla} | \Phi_t \rangle|^2 \rho_b(E_{\vec{k}}) , \qquad (4.1)$$

and $h\nu = E^0 + E_{\vec{k}}$, where E^0 is the optical ionization energy. $\rho_b(E_{\vec{k}})$ represents the number of states with energy $E_{\vec{k}}$ in band b, $|b, \vec{k}\rangle$ the corresponding electronic wave function, approximated by the unperturbed crystal Bloch function. Finally, Φ_t is the electronic wave function for the system with an electron trapped on the level.

If one considers the level as being built up from only b' band states,

$$\Phi_t = \sum_k A_{\vec{k}} |b', \vec{k}\rangle , \qquad (4.2)$$

Eq. (4.1) becomes

$$\sigma^{el}(h\nu) \propto \frac{1}{h\nu} A_{\vec{k}}^2 |\langle b, \vec{k} | -i\hbar\vec{\nabla} | b', \mathrm{k}\rangle|^2 \rho_b(E_{\vec{k}}) . \quad (4.3)$$

This expression shows that the spectral shape of $\sigma^{el}(h\nu)$ depends on three physical characteristics: the $A_{\vec{k}}$ coefficients of the expansion of the impurity wave function Φ_t in terms of the relevant Bloch functions, the matrix element between Bloch states $\langle b, \vec{k} | -i\hbar\vec{\nabla} | b', \vec{k}\rangle$, and the density of states in the continuum $\rho_b(E_{\vec{k}})$. One must add the Franck-Condon parameter d_{FC} which, for a level with a given thermal ionization energy, determines the optical ionization energy E^0; d_{FC} also accounts for the temperature dependence of the $\sigma^0(h\nu)$ spectra. The various combinations of the possible hypothesis one can make concerning each of these points lead to the different existing theoretical models.

The $A_{\vec{k}}$ components are generally calculated using plane waves instead of Bloch states in Eq. (4.2). $A_{\vec{k}}$ thus appears as the Fourier transform of Φ_t. This explains very simply why the optical cross-section spectra are broader for deep levels (localized wave function) than for shallow levels (delocalized wave function), and accounts for the use in most of the models of a wave function derived from a δ-type potential $[\Phi_t(r) \propto \exp(-\alpha r)/r,\ A_{\vec{k}} \propto (k^2+\alpha^2)^{-1}]$, as introduced by Lucovsky.[65]

For a given Φ_t wave function, $A_{\vec{k}}$ still depends on α, which controls its extent. This parameter is commonly written in the effective-mass approximation as a function of E^0 and the effective-mass $m^*_{b'}$ $(\alpha^2 = 2m^*_{b'}E^0/\hbar^2)$, thus leading to a distinction between photoionization $(b=b')$ and photoneutralization $(b \neq b')$ spectra, the ratio m^*_c/m^*_v of the effective masses in the CB and valence band (VB) appearing in the latter [since $k^2 = 2m^*_b(h\nu - E^0)/\hbar^2$].[8]

The matrix element $\langle b,\vec{k}\,|-i\hbar\vec{\nabla}|\,b',\vec{k}\rangle$, which will be denoted $\langle\vec{k}|\vec{p}|\vec{k}\rangle$, also depends on the nature of the investigated transition: photoionization or photoneutralization. Indeed, using $|b,\vec{k}\rangle = u_{b,\vec{k}}(\vec{r}) \times \exp(i\vec{k}\cdot\vec{r})$, this matrix element becomes[8]

$$\langle\vec{k}|\vec{p}|\vec{k}\rangle = -i\hbar \int u^*_{b,\vec{k}}(\vec{r})\,\vec{\nabla} u_{b',\vec{k}}(\vec{r})\,d\vec{r} + \hbar\vec{k}\int u^*_{b,\vec{k}}(\vec{r})\,u_{b',\vec{k}}(\vec{r})\,d\vec{r}\,. \tag{4.4}$$

In the case of photoionization $(b=b')$, the first integral in Eq. (4.4) vanishes; we end up with a term proportional to $\hbar\vec{k}$, a forbidden dipole transition. In the case of photoneutralization $(b\neq b')$, the transition takes place between states with different symmetries. Consequently, the first term in Eq. (4.4) is finite, while the second vanishes: This gives a constant matrix element independent of $\vec{k}$, an allowed transition. Such a constant matrix element has been used by Kopylov and Pikhtin[66] and others[8,11,67] to account for narrower experimental spectra than predicted by Lucovsky's model.

These two opposite forms for the matrix element, $\langle\vec{k}|\vec{p}|\vec{k}\rangle = \text{const}$ and $\langle\vec{k}|\vec{p}|\vec{k}\rangle \propto \vec{k}$, are the most commonly used in analytical models. However, they represent two very crude approximations as soon as one is interested in transitions towards states lying farther from the band edge, i.e., in the spectral shape of the optical cross sections far from the thresholds. A more realistic calculation would require to make allowance for the $\vec{k}$ dependence of the integrals in Eq. (4.4), which is only possible through a numerical evaluation using the real band structure. Such approaches have been made by Jaros[68] and Pantelides,[69] but their results could not be tested, due to the lack of experimental information over a large photon energy range. Jaros[44] also proposed an analytical model to account for such effects; however, its practical interest seems to be limited by the presence of two badly known parameters, one of which having a drastic influence on the spectra (see Fig. 5 in Ref. 44).

The crystal band structure is also involved in Eq. (4.3) through the density-of-states term $\rho_b(E_{\vec{k}})$. Most of analytical models use the one-band parabolic approximation here; only Grimmeiss[70] raises problems due to the nonparabolicity and nonsphericity of the valence band in silicon. Jaros[44] also mentions the crudeness of this approximation in the case of the GaAs conduction band, due to the low density-of-states area near Γ, but he does not introduce any more general expression in his analytical model.

We have tried to use the above-mentioned models to account for the spectral distribution of the optical cross sections obtained through DLOS. However, we rapidly found that neither could fit the experimental curves over the whole photon energy range investigated. This is quite obvious in the case of transitions to CB, since all these models use a unique conduction-band minimum, whereas all the experimental spectra clearly show a complex structure. But this also concerns transitions to the VB, as demonstrated in Fig. 19 for the "oxygen" level. We have reported in this figure the best adjustments of our experimental $\sigma^0_p(h\nu)$ curve using Kopylov-Pikhtin's and Lucovsky's models; neither predicts the large signal drop between 0.95 and 1.1 eV. This example clear-

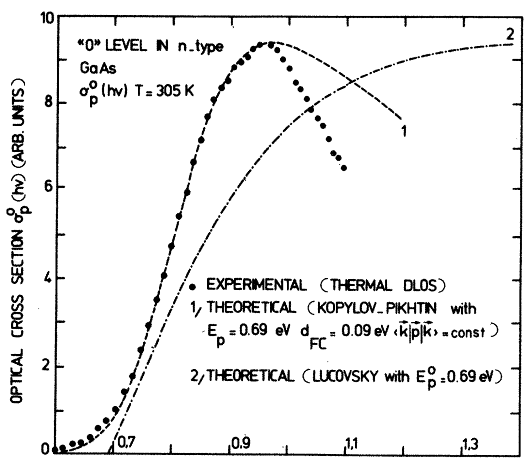

FIG. 19. An illustration of the failure of commonly used theoretical models to account for the DLOS determined optical cross sections spectra over a large photon energy range. Neither of Kopylov-Pikhtin's (curve 1) or Lucovsky's (curve 2) models predicts the large drop above 0.95 eV of the "O" level $\sigma^0_p(h\nu)$ cross section, as experimentally observed (thermal DLOS •).

ly demonstrates the importance of the large photon energy range investigated. Indeed, in the absence of the decreasing part of the experimental curve, we would have wrongly concluded that there is good agreement with one of the models. In fact, almost any model can be fitted to any $\sigma^0(h\nu)$ experimental curve using an adjustable d_{FC} parameter as soon as the available information stops at the maximum of the curve. Thus it seems vain to apply sophisticated models in such cases.

Another essential condition for a reliable test of theoretical models is that both $\sigma_n^0(h\nu)$ and $\sigma_p^0(h\nu)$ cross sections are experimentally available. Indeed, the model must then simultaneously account for both spectra, using the same set of physical parameters concerning the level (wave function, lattice relaxation).

B. Theoretical model

The failure of previously reported models undoubtedly arises from the lack of experimental techniques able to provide both $\sigma_n^0(h\nu)$ and $\sigma_p^0(h\nu)$ spectra over a large photon energy range. We have thus been involved in the work of computing a model able to take advantage of this newly available experimental information. Because of the poor general understanding in deep-level physics at the present time, our aim has been to develop a general but as simple as possible expression, without using complicated wave functions, minimizing the number of adjustable parameters. We have used the following physical hypotheses.[30,71]

(a) The impurity potential is represented by a Dirac well.

(b) The bound-state wave function is written in the effective-mass approximation $[r^{-1}\exp(-\alpha r)]$, but its extent α^{-1} is taken as a fitting parameter. From a physical point of view, this is equivalent to proposing an adjustable "effective mass" for the trapped electron to account for the admixture of both conduction-band and valence-band states in the deep-level formation.

(c) The band structure is approximated by a series of parabolic bands, localized on its different extrema i, using the proper effective masses m_i^*.

(d) The $\sigma^0(h\nu)$ spectrum is considered as the superposition of the elementary $\sigma_i^0(h\nu)$ spectra corresponding to transitions to the various valleys, weighted by the number of equivalent extrema M_i and by an adjustable coefficient P_i representing the oscillator strength of the transition to each minimum.

(e) The matrix element is supposed to keep the same form over the whole photon energy range. Two limiting cases are considered: forbidden ($\langle\vec{k}|\vec{p}|\vec{k}\rangle \propto \vec{k}$) and allowed ($\langle\vec{k}|\vec{p}|\vec{k}\rangle = \text{const}$) transitions.

(f) The electron-phonon interaction is taken into account in the event of strong phonon coupling.[44,66,67]

Following Eq. (4.3), the electronic matrix element for the transition towards extremum i of the band can be written as

$$\sigma_i^{el}(h\nu) \propto P_i M_i \frac{1}{h\nu}\frac{1}{(k^2+\alpha^2)^2} k^{2a} m_i^{*3/2}(h\nu - E^0 - \Delta i)^{1/2} \tag{4.5}$$

with $a=0$ for an allowed transition, $a=1$ for a forbidden transition; Δi is the energy difference between extrema i and Γ of the band. Let us note that this expression can be immediately generalized to Coulomb-type wells through

$$\sigma_i^{el}(h\nu) \propto \frac{P_i M_i m_i^{*3/2}}{h\nu}\frac{k^{2a}}{(k^2+\alpha^2)^{2b}}(h\nu - E^0 - \Delta i)^{1/2} \tag{4.6}$$

with $b=1$ for a Dirac well, $b=2$ for a Coulomb well. Using $h\nu = E^0 + \Delta i + \hbar^2 k^2/2m_i^*$, Eq. (4.6) becomes

$$\sigma_i^{el}(h\nu) \propto P_i M_i (m_i^*)^{a-2b+3/2}\frac{1}{h\nu}\frac{(h\nu - E^0 - \Delta i)^{a+1/2}}{[(h\nu - E^0 - \Delta i) + \hbar^2\alpha^2/2m_i^*]^{2b}}. \tag{4.7}$$

The cross section can be written as a function of the normalized photon energy $y = h\nu/E^0$,

$$\sigma_i^{el}(y) \propto P_i M_i c_i^{2b-a-3/2}\frac{1}{y}\frac{(y-1-\Delta i/E^0)^{a+1/2}}{[(y-1-\Delta i/E^0)+mc_i]^{2b}}, \tag{4.8}$$

with $m = \hbar^2\alpha^2/2m_\Gamma^* E^0$ and $c_i = m_\Gamma^*/m_i^*$. Including the electron-phonon interaction,[44] the optical cross section for the transition towards extremum i becomes

$$\sigma_i^0(y) \propto \frac{1}{y\Theta^{1/2}} P_i M_i c_i^{2b-a-3/2} \times \int_{1+\Delta i/E^0}^{\infty} \frac{(x-1-\Delta i/E^0)^{a+1/2}}{[(x-1-\Delta i/E^0)+mc_i]^{2b}} \times \exp\left(-\frac{(y-x)^2}{\Theta}\right)dx \tag{4.9}$$

where $\Theta = 4kTd_{FC}/E^{0 2}$ is the temperature-dependent parameter. Finally, the total optical cross section is given by the following analytical expression:

$$\sigma^0(y) \propto \frac{1}{y\Theta^{1/2}} \sum_i P_i M_i c_i^{2b-a-3/2} \times \int_{1+\Delta i/E^0}^{\infty} \frac{(x-1-\Delta i/E^0)^{a+1/2}}{[(x-1-\Delta i/E^0)+mc_i]^{2b}} \times \exp\left(-\frac{(y-x)^2}{\Theta}\right)dx, \tag{4.10}$$

where the summation is extended to the different extrema of the band. It should be pointed out that Eq. (4.10) allows one to come back to the one-parabolic band simplified model, taking $P_i = M_i = c_i = 1$ and $\Delta i = 0$. One can then easily check that the expressions corresponding to most of the previously mentioned photoionization and photoneutralization models are immediately obtained replacing, in m, α^2 by its expression in the effective-mass approximation.

The last expression is very general, since it applies for Dirac- or Coulomb-type potentials, allowed or forbidden transitions, and for any material. We have taken $b=1$ here, since the localization of the impurity potential associated with a deep state is certainly better accounted for by a Dirac well. Furthermore, the first comparison with experimental results led us to conclude that the sharpness of the $\sigma^0(h\nu)$ spectra could only be understood assuming allowed transitions ($a=0$). This is easily understood, since due to the admixture of conduction- and valence-band states in the deep-level formation, the optical cross sections can be seen as the superposition of allowed and forbidden terms, the allowed one being indeed always dominant. We have thus used the following relation:

$$\sigma^0(y) \propto \frac{1}{y\Theta^{1/2}} \sum_i P_i M_i c_i^{1/2} \times \int_{1+\Delta i/E^0}^{\infty} \frac{(x-1-\Delta i/E^0)^{1/2}}{[(x-1-\Delta i/E^0)+mc_i]^2} \times \exp\left(-\frac{(y-x)^2}{\Theta}\right) dx \qquad (4.11)$$

Coefficients M_i and m_i^* (which appears in c_i) and Δi suitable for GaAs have been found in the literature. For the conduction band, we have used a three-band parabolic approximation, using Aspnes's experimental results[72]; the relevant values for all coefficients have been summarized in Table IV. This approximation is well justified, even far enough from the band edge; this can be checked using the GaAS band structure, as obtained from pseudopotential calculations.[73] Figure 20, which

TABLE IV. Three-band parabolic approximation used for the GaAs conduction band. The values of coefficients m_i^*, Δi, and M_i ($i = \Gamma, L, X$) are borrowed from Aspnes's experimental results (Ref. 72).

i	m_i^*	c_i	Δi	M_i
Γ	$0.067m_0$	1	0	1
L	$0.22m_0$	0.30	0.29 eV	4
X	$0.41m_0$	0.16	0.46 eV	3

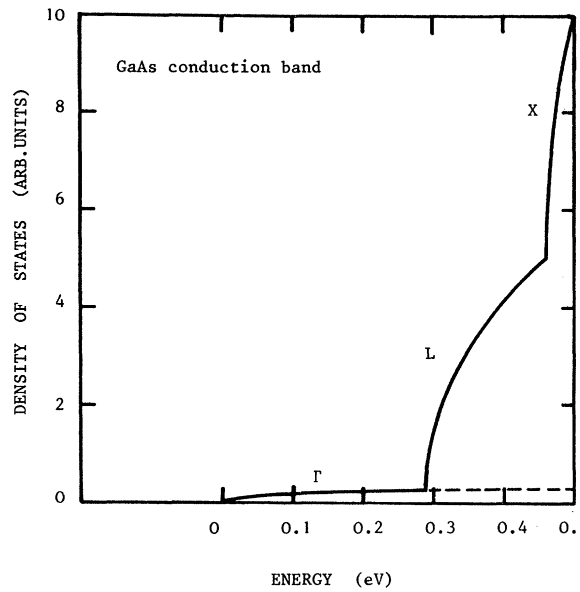

FIG. 20. GaAs conduction-band density-of-states distribution in the three-band parabolic approximation used in this work (solid line), as compared to the classical approximation (dashed lines). The high density of states regions lying 0.29 eV (L) and 0.46 eV (X) above the Γ fundamental minimum cannot be neglected as far as the higher energy parts of the $\sigma_n^0(h\nu)$ curves are concerned.

represents the corresponding CB density of states, clearly shows the inadequacy of the one-band parabolic approximation as far as the higher energy parts of the $\sigma_n^0(h\nu)$ curves are concerned. We have used the one-band approximation for the valence band, using a $m_v^* = 0.54m_0$ resultant effective mass.[74]

Finally, there remains only three adjustable physical parameters in Eq. (4.11): the bound-state wave function extent α^{-1}, through m; the Franck-Condon parameter d_{FC}, through Θ and E^0 [E^0 is not an additional parameter, since it is directly related to d_{FC} and to the binding energy E ($E^0 = E + d_{FC}$) determined through thermal spectroscopy], the relative P_i ($i = \Gamma, L, X$) oscillator strengths (normalized to P_Γ).

Figure 21 shows the influence of m (or α) on the $\sigma_p^0(h\nu)$ curve given by Eq. (4.11). It can be seen that this parameter controls the width of the spectrum, and especially the location of its maximum, whereas the position and the shape of the threshold are quite unchanged. The observed enlargement while m is increased is due to the corresponding enhanced localization of the trapped electron wave function ($\alpha^{-1} \propto 1/\sqrt{m}$). The influence of d_{FC} on the same $\sigma_p^0(h\nu)$ curve appears in Fig. 22. The main effect is the displacement of the transition threshold, the general shape of the curve being almost

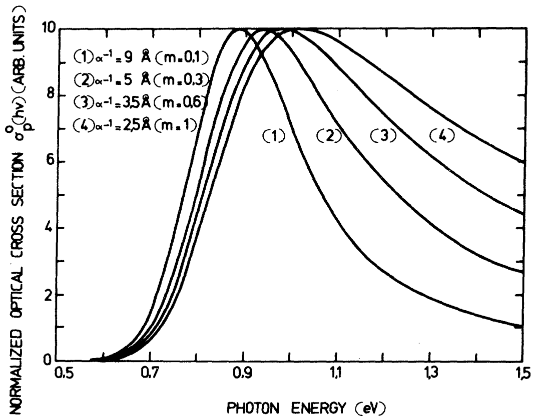

FIG. 21. Influence of the bound-state wave-function extent α^{-1} (through m) on the theoretical $\sigma^0(h\nu)$ curve given by Eq. (4.11). We have considered here transitions between the valence band ($P_i = M_i = c_i = 1$, $\Delta i = 0$) and a level characterized by $E_p = 0.69$ eV and $d_{FC} = 0.12$ eV at 300 K ($\Theta = 1.9 \times 10^{-2}$). The width of the spectrum appears to be very sensitive to this parameter.

insensitive to this parameter. The coefficients P_i just modify the relative contributions of the different CB extrema in the $\sigma_n^0(h\nu)$ curves.

This simulation clearly shows that the three adjustable parameters have well-characterized effects on the spectra, so that the relevant physical quantities can be unambigously extracted from the experimental results. It should be emphasized that the $\sigma_p^0(h\nu)$ experimental curves are of prime interest for such an adjustment, since they are

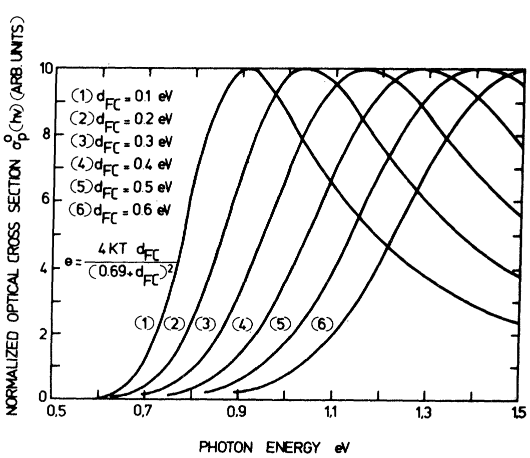

FIG. 22. Influence of the Franck-Condon parameter d_{FC} (trough $E°$ and Θ) on the theoretical $\sigma^0(h\nu)$ curve given by Eq. (4.11). We have considered here transitions between the valence band ($P_i = M_i = c_i = 1$, $\Delta i = 0$) and a level characterized by $E_p = 0.69$ eV and $\alpha^{-1} = 5$ Å at $T = 300$ K. It can be seen that this parameter mainly controls the position of the transition threshold.

required to determine α^{-1} with good accuracy. Indeed, due to the low effective mass m_Γ^* near the Γ minimum of CB, the $\sigma_\Gamma^0(h\nu)$ contribution to $\sigma_n^0(h\nu)$ is always very broad (large m). As a consequence, its decreasing part and even its maximum, from which α^{-1} is obtained, are masked by the transitions towards upper minima.

C. Theoretical fit of the DLOS results—discussion

The "oxygen" level constitutes a very good test for our theoretical expression, since both $\sigma_n^0(h\nu)$ and $\sigma_p^0(h\nu)$ are available from DLOS over a large photon energy range. We have plotted in Fig. 2 the theoretical curve adjusted to the $\sigma_p^0(h\nu)$ spectrum obtained at room temperature; we introduced the $E_p = 0.69$ eV thermal ionization energy, as deduced from DLTS results. The theoretical spectrum, using $d_{FC} = 0.12$ ev ($E_p^0 = 0.81$ eV, $\Theta \sim 2 \times 10^{-2}$) and $m_p = 0.35$, is in very good agreement with the experimental one, up to around 1.1 eV. The increase of the optical cross section observed above this energy must be associated with an increase in the effective VB density of states with respect to the single parabolic approximation used here. It should be pointed out that the small feature near 0.9 eV, systematically observed on the "O" level $\sigma_p^0(h\nu)$ spectrum, might be related to transitions to the split-off valence band ($E_v - 0.3$ eV). If one uses the values of d_{FC} and α^{-1} deduced from the previous adjustment, the only adjustable parameters for fitting the $\sigma_n^0(h\nu)$ curve are the relative transition probabilities P_i. A good fit is obtained for $P_L = 0.25$ and $P_X = 0.1$, as shown on Fig. 6. The values of the other quantities are $d_{FC} = 0.12$ eV ($\Theta = 5 \times 10^{-3}$), $m_n = 2.5$ (which corresponds to $m_p = 0.35$), and $E_p^0 = 0.86$ eV.

A similar analysis has been carried out for the $\sigma_n^0(h\nu)$ experimental curve of defect $E3$. Figure 13 shows the best theoretical adjustment, corresponding to $E_n^0 = 0.44$ eV ($\Theta \sim 4 \times 10^{-2}$, $d_{FC} \sim 0.2$ eV), $m_n = 2$, $P_L = 0$, and $P_X = 0.15$. Rather good agreement is obtained, except around 0.85 eV where the measured optical cross section is larger than that predicted by the model. We noted that it was impossible to get a better adjustment while involving transitions towards extremum L ($P_L \neq 0$), the threshold of which would lie near 0.6 eV, and this explains why we kept $P_L = 0$.

We have also applied this model to our results concerning level $EL1$. We concluded that such a model could not account for the sharpness of the $\sigma_n^0(h\nu)$ DLOS spectrum (Fig. 9), thus confirming the previous assessment that internal transitions are involved.[3] Transitions towards Γ are likely to be masked by these internal transitions, as suggested by the increase in the DLOS signal above

1 eV, probably associated to transitions toward upper minima.

The physical parameters deduced from the previous adjustments are summarized on Table V; also indicated in this table are the estimated trapped electron "effective" masses calculated from $\alpha^2 = 2m^*E/\hbar^2$. For *EL*6, *EL*3, and Cu levels, we only give the Franck-Condon parameter d_{FC} deduced from a comparison between thermal and optical ionization energies, the last one being taken at the inflection point of the $\sigma_n^0(h\nu)$ curves.

It can be seen that the bound-state wave-function extent α^{-1} does not change very much from one level to another; the mean value, 5 Å, is consistent with theoretical calculations[44] and with the simplest idea of a deep-state defect. Besides, transitions to the Γ minimum of CB seem to be the most probable in GaAs, even if the contributions of upper L and X minima to the $\sigma_n^0(h\nu)$ curves are always very important, due to a much higher density of states. Indeed, this result is in a fair agreement with White's qualitative conclusions, as deduced from DSDP investigations.[2,17] The relative importance of the transitions to L and X depends on the level (in particular, no transitions to L seem to occur in the case of *E*3), which is likely to be due to the different symmetries of the related defects.

Table V also indicates that the most common value for the Franck-Condon parameter d_{FC} is 0.1–0.2 eV in GaAs. Figures 23 and 24 show the configuration coordinate (CC) diagrams obtained for "O" and *E*3 levels. The "O" diagram cannot account for the 80-meV thermal activation energy measured by Lang for the electron-capture cross section.[34] If this value really corresponds to the multiphonon emission (MPE) mechanism, it indicates the roughness of the simple harmonic approximation used here. The dashed curve in Fig. 23 represents the metastable state of the "oxygen" center, which is responsible for the previously reported photocapacitance quenching effect.[38,39] Figure 24 shows that the ground state of *E*3 also belongs to this "normal" lattice relaxation group, even if the curve corresponding to the electron trapped on the level cannot be positioned very precisely, due to uncertainties in the binding energy determination (electric field effects[62]). This result is not in agreement with the hypothesis of Lang, who proposed a large lattice relaxation effect to explain the large hole-capture cross section of the level. Indeed, the simple CC diagram in Fig. 24 cannot explain such a large σ_p and the recombination enhanced motion as proposed by Lang.[59] However, a large relaxation would yield a very different $\sigma_n^0(h\nu)$ spectrum, enlarged and shifted to higher energies, and is therefore ruled out by the DLOS result. The only way to reconcile all these observations is to assume a more complex CC diagram. Nevertheless, the minimum of the curve $(E3+e^-)$ in Fig. 24 cannot be modified in view of our experimental result.

The most striking result in Table V is probably the 0.6-eV Franck-Condon parameter found for *EL*6. Figure 25 shows the corresponding CC diagram. The large lattice relaxation effect explains the high value of the $\sigma_n^0(h\nu)$ threshold energy and the absence of any optical refilling from the valence band as experimentally observed. Let us note that this diagram is very similar to the one proposed by Lang[27,28] to account for persistent photoconductivity effects in $Al_xGa_{1-x}As$. In the present case, the elastic barrier height for the capture of an electron on the level is lower. However, such a CC diagram predicts that the persistent photoconductivity effect might arise for this *EL*6 defect which is frequently present in bulk GaAs. Anyway, *EL*6 must be classified as a defect with strong lattice relaxation as *DX* in $Al_xGa_{1-x}As$ (Ref. 28), O in GaP (Ref. 26), "O" in GaAs (Ref. 39), or S in $GaAs_{1-x}P_x$ (Ref. 75).

V. SUMMARY AND CONCLUSIONS

A transient photocapacitance technique has been described. It allows a true deep-level optical

TABLE V. Physical parameters deduced from a coupled DLTS-DLOS analysis of the main deep levels in GaAs.

Level	Experimental activation energy (eV)	α^{-1} (Å)	P_L/P_Γ	P_X/P_Γ	d_{FC} (eV)	Binding energy (eV)	Trapped electron "effective mass"
O (*EL*2)	0.80	5	0.25	0.1	0.12	0.74 (E_n)	$0.2m_0$
*E*3	0.31	8	0	0.15	0.2	0.24 (E_n)	$0.26m_0$
*EL*6	0.31				~0.6	~0.3 (E_n)	
*EL*1	0.76				?	0.72 (E_p)	
*EL*3	0.44				~0.05	~0.44 (E_n)	
Cu (*HL*4)	0.40				~0	0.40 (E_p)	

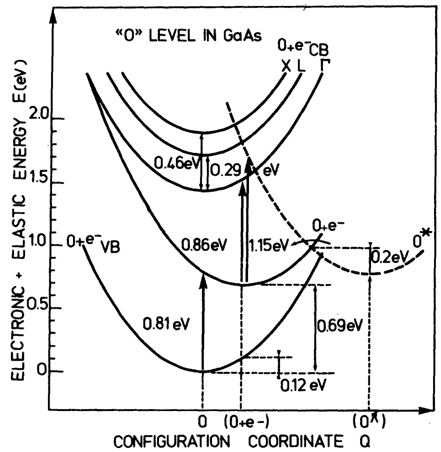

FIG. 23. Configuration coordinate diagram for the "oxygen" level in GaAs, as obtained from DLTS and DLOS results. The dashed curve represents the very large relaxation metastable state of the "oxygen" center responsible for the photocapacitance quenching effect.

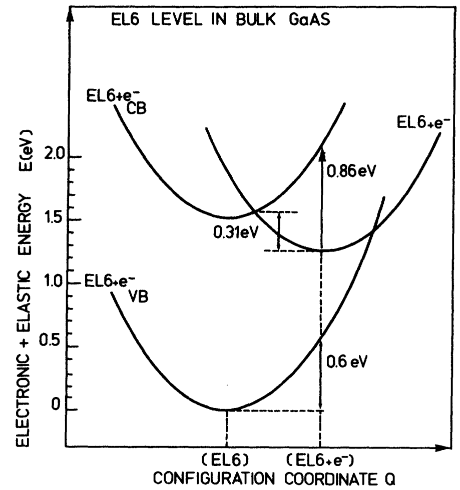

FIG. 25. Configuration coordinate diagram for $EL6$ in bulk GaAs. The large difference between the optical ionization energy and thermal activation energy, as given by DLOS and DLTS, as well as the lack of any optical refilling from the valence band, are two consequences of the large lattice relaxation effect taking place on the center.

spectroscopy, i.e., direct independent measurements of both $\sigma_n^0(h\nu)$ and $\sigma_p^0(h\nu)$ optical cross sections involving each trap and the conduction and valence bands, respectively. The basic idea of the method is to use the initial derivative of the photocapacitance transients, which is directly proportional to σ_n^0 or σ_p^0, provided that the proper initial condition, i.e., all centers filled with electrons or holes has been reached in the level. The spectral distribution of the optical cross section is thus directly obtained by recording this derivative, after suitable averaging and corrections, while the photon energy is scanned. The various DLOS modes of operation, in which the initial conditions are reached through electrical, thermal, or optical excitation, have been described.

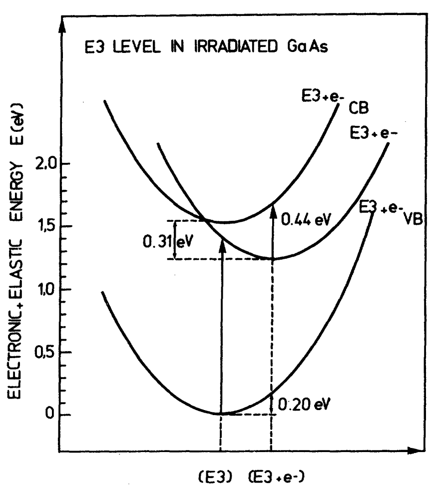

FIG. 24. Configuration coordinate diagram for $E3$ in irradiated GaAs. The CC curve for the electron trapped on the level has been positioned using the 0.44-eV optical ionization energy (DLOS) and the 0.31-eV thermal activation energy (DLTS). Even if the latter value can be discussed with respect to electric field effects, the DLOS result clearly indicates that this level belong to the "normal" lattice relaxation group.

This experimental method has been used to analyze the optical properties of the most commonly observed deep levels in n-type GaAs: the so-called "oxygen" level, the copper-related hole trap, the deep $EL1$ level in chromium-doped material, the dominant electron trap $EL6$ in bulk samples, and the radiation-damage level $E3$. Each trap was first characterized by its thermal "signature," i.e., thermal ionization energy and capture cross section. This was done through usual DLTS measurements carried out on the same sample and apparatus as used for DLOS. When several levels were present in a given sample, their optical responses were experimentally separated using the selectivity of DLOS, as described in the text, for e.g., the radiation damage level $E3$, the response of which was isolated from those of the other radiation induced levels, namely $E4$ and $E5$.

DLOS was used to analyze both $\sigma_n^0(h\nu)$ and $\sigma_p^0(h\nu)$ spectra from their energy thresholds up to the energy gap of the material. It should be emphasized that this method insures no mixing of the two optical cross sections over all the relevant spectral range, even for mid gap levels, such as the "oxygen" level with a $E_n = 0.75$ eV thermal binding energy. This was not verified for the previously used experimental methods, such as optical absorption, photoconductivity, or related techniques. This large photon energy range over which the $\sigma_n^0(h\nu)$ and $\sigma_p^0(h\nu)$ curves were determined allowed two main observations.

(i) A well-defined structure can be resolved in all $\sigma_n^0(h\nu)$ spectra. It is suggested that this structure reflects the density of states distribution in the GaAs conduction band. This is the first direct observation of transitions towards the various valleys Γ, L, and X of this band. On the basis of this interpretation, it has been possible to reinterpret most of the previously reported measurements on the "oxygen" level, using either photocapacitance or double source differentiated photocapacitance, optical absorption or photoconductivity. It was shown that very good agreement can therefore be obtained among the numerous works reported for this particular deep level.

(ii) All $\sigma^0(h\nu)$—especially $\sigma_p^0(h\nu)$—spectra appear to be much sharper than predicted by the commonly used Lucovsky's model.

In order to deduce quantitative conclusions from this newly available experimental information, we have developed a simple phenomenological model, including a reduced number of adjustable parameters: (i) the bound-state envelope wave-function extent α^{-1} (in the δ-potential approximation) which accounts for the admixture of both conduction-band and valence-band states in the deep-level formation, (ii) the relative transition probabilities P_i to Γ, L, and X conduction-band minima (taken in the three-band parabolic approximation), and (iii) the Frank-Condon parameter d_{FC} which represents the electron-phonon interaction. These parameters have been shown to have well distinguishable effects on the spectra so that the relevant physical quantities could be unambiguously extracted from the experimental results. It should be emphasized that the knowledge of both $\sigma_n^0(h\nu)$ and $\sigma_p^0(h\nu)$ optical cross-section spectra provides a very crucial test for any theoretical model. Nevertheless, it has been possible to fit both $\sigma_n^0(h\nu)$ and $\sigma_p^0(h\nu)$ for the "oxygen" level over a very large photon energy range using, indeed, a unique set of parameters. This was generally not done before.

From this first theoretical analysis of DLOS results, it turns out that (i) the sharpness of all $\sigma^0(h\nu)$ spectra can be understood if allowed optical transitions are assumed, which probably arises form the admixture of conduction and valence band states in any deep level formation, (ii) the bound-state envelope wave-function extent is generally about 5 Å, in agreement with recent theoretical calculations and with intuitive concept, (iii) transitions to the Γ minimum of the conduction band are always the most probable, even if their contribution to the $\sigma_n^0(h\nu)$ curves is weak, due to the low density of states in this region, and (iiii) the relative transition probabilities P_L/P_Γ and P_X/P_Γ change from one level to another, which is likely to be related to the relevant defect symmetries.

The values of the Franck-Condon parameter d_{FC} were generally found in the 0.1–0.2 eV range. The radiation-damage level $E3$ was shown to belong to this "normal" lattice relaxation group. Only the copper-related hole trap appeared to have a zero d_{FC}, whereas a new example of large lattice relaxation centers was discovered, $EL6$ in bulk material. The thermal activation energy for electron emission is 0.31 eV, while the optical ionization energy E_n^0 is about 0.85 eV, thus leading to $d_{FC} \sim 0.6$ eV. Indeed, the DLOS method used in this work allows an unambigous identification of the thermal and optical responses of a particular center. This would be quite impossible for such large lattice relaxation centers using usual methods.

As a conclusion, the DLOS measurements described in this work have brought the photocapacitance method to the stage where it is not only a nice technique for optical characterization of semiconducting materials, but also a valuable tool for the study of the physics of deep-level defects.

ACKNOWLEDGMENTS

The authors are indebted to LEP (Laboratoires d'Electronique et de Physique Appliquée, Paris) and RTC (Radiotechnique Compelec, Caen) for supplying the samples used in this work.

[1]A. Mircea and D. Bois, in *International Conference on Radiation Effects in Semiconductors Nice, 1978*, edited by J. H. Albany (Institute of Physics, London, 1979), p. 82.

[2]A. M. White, P. Porteous, W. F. Sherman, and A. A. Stadtmuller, J. Phys. C 10, L473 (1977).

[3]D. Bois and P. Pinard, Phys. Rev. B 9, 4171 (1974).

[4]G. K. Ippolitova, E. M. Omel'Yanovskii, and L. Y. Pervova, Fiz. Tekh. Poluprovodn. 9, 1308 (1975) [Sov. Phys.—Semicond. 9, 864 (1976)].

[5]G. M. Martin, M. L. Verheÿke, J. A. J. Jansen, and G. Poiblaud, J. Appl. Phys. 50, 467 (1979).

[6]H. J. Stocker and M. Schmidt, J. Appl. Phys. 47, 2450 (1976).
[7]E. C. Lightowlers and C. M. Penchina, J. Phys. C 11, L405 (1978).
[8]B. Monemar and L. Samuelson, Phys. Rev. B 18, 809 (1978).
[9]L. Samuelson and B. Monemar, Phys. Rev. B 18, 830 (1978).
[10]H. G. Grimmeiss and L. Å. Ledebo, J. Appl. Phys. 46, 2155 (1975).
[11]E. H. Tyler, M. Jaros, and C. M. Penchina, Appl. Phys. Lett. 31, 208 (1977).
[12]Y. Furukawa, Jpn. J. Appl. Phys. 6, 675 (1967).
[13]A. A. Gutkin, A. A. Lebedev, R. K. Radu, G. N. Talalakin, and T. A. Shaposhnikova, Fiz. Tekh. Poluprovodn. 5, 1954 (1972) [Sov. Phys.—Semicond. 6, 1674 (1973)].
[14]K. Sakai and T. Ikoma, Appl. Phys. 5, 165 (1974).
[15]D. Bois, J. Phys. F 35, C3, 241 (1974).
[16]R. Legros, Y. Marfaing, and R. Triboulet, J. Phys. Chem. Solids 39, 179 (1978).
[17]A. M. White, P. J. Dean and P. Porteous, J. Appl. Phys. 47, 3230 (1976).
[18]H. Kukimoto, C. H. Henry, and F. R. Merritt, Phys. Rev. B 7, 2486 (1973).
[19]C. H. Henry, H. Kukimoto, G. L. Miller, and F. R. Merritt, Phys. Rev. B 7, 2499 (1973).
[20]D. V. Lang, J. Appl. Phys. 45, 3023 (1974).
[21]A. Mitonneau, G. M. Martin, and A. Mircea, in International Symposium on GaAs and Related Compounds, Edinburgh, 1976 (unpublished).
[22]C. Hurtes, M. Boulou, A. Mitonneau, and D. Bois, Appl. Phys. Lett., 32, 821 (1978).
[23]H. Lefevre and M. Schulz, Appl. Phys. 12, 45 (1977).
[24]G. L. Miller, D. V. Lang, and L. C. Kimerling, Ann. Rev. Mater. Sci. 1977, 377.
[25]C. T. Sah, L. Forbes, L. L. Rosier, and A. F. Tasch, Solid State Electron., 13, 759 (1970).
[26]C. H. Henry and D. V. Lang, Phys. Rev. B 15, 989 (1977).
[27]D. V. Lang and R. A. Logan, Phys. Rev. Lett. 39, 635 (1977).
[28]D. V. Lang, R. A. Logan, and M. Jaros, Phys. Rev. B 19, 1015 (1979).
[29]D. Bois, A. Chantre, G. Vincent, and A. Nouailhat, in *Proceedings of the 14th International Conference on the Physics of Semiconductors, Edinburgh, 1978,* edited by B. L. H. Wilson (Institute of Physics, Bristol, 1978), p. 295.
[30]A. Chantre, Ph.D. thesis, Grenoble, 1979 (unpublished).
[31]G. Vincent, Appl. Phys. 23, 215 (1980).
[32]H. G. Grimmeiss, L. Å. Lebedo, and E. Meijer, in 2nd "Lund" International Conference on Deep Level Impurities in Semiconductors, Ste. Maxime, 1979 (unpublished).
[33]A. Chantre, G. Vincent, G. Guillot, and D. Bois, in 2nd "Lund" International Conference on Deep Level Impurities in Semiconductors, Ste. Maxime, 1979 (unpublished).
[34]D. V. Lang and R. A. Logan, J. Electron Mater. 4, 1053 (1975).
[35]G. M. Martin, A. Mitonneau, and A. Mircea, Electron. Lett. 13, 191 (1977).
[36]D. Bois and M. Boulou, Phys. Status Solidi A 22, 671 (1974).
[37]A. Mircea, A. Mitonneau, J. Hallais, and M. Jaros, Phys. Rev. B 16, 3665 (1977).
[38]D. Bois and G. Vincent, J. Phys. F 38, L351 (1977).
[39]G. Vincent and D. Bois, Solid State Commun. 27, 431 (1978).
[40]A. Zylbersztejn, R. H. Wallis, and J. M. Besson, Appl. Phys. Lett. 32, 764 (1978).
[41]A. Mircea and A. Mitonneau, J. Phys. 40, L31 (1979).
[42]H. J. Stocker, J. Appl. Phys. 48, 4583 (1977).
[43]S. F. Ross and M. Jaros, Phys. Lett. 45A, 355 (1973).
[44]M. Jaros, Phys. Rev. B 16, 3694 (1977).
[45]A. Humbert, L. Hollan, and D. Bois, J. Appl. Phys. 47, 4137 (1976).
[46]A. M. Huber, N. T. Linh, J. C. Debrun, M. Valladon, G. M. Martin, A. Mitonneau, A. Mircea (unpublished).
[47]G. Vincent, Ph. D. thesis, Lyon, 1978 (unpublished).
[48]A. Mircea and A. Mitonneau, Appl. Phys. 8, 15 (1975).
[49]F. Hazegawa and A. Majerfeld, Electron. Lett. 11, 286 (1975).
[50]S. S. Chiao, B. L. Mattes, and T. H. Bube, J. Appl. Phys. 261 (1978).
[51]U. Kaufmann and J. Schneider, Solid State Commun. 20, 143 (1976).
[52]J. J. Krebs and G. H. Stauss, Phys. Rev. B 15, 17 (1977).
[53]A. L. Lin and R. H. Bube, J. Appl. Phys. 47, 1859 (1976).
[54]C. I. Huang and S. S. Li, Solid State Electron. 16, 1481 (1973).
[55]G. Vincent, A. Chantre, and D. Bois, J. Appl. Phys. 50, 5484 (1979).
[56]D. Pons, A. Mircea, A. Mitonneau, and G. M. Martin, in *International Conference on Radiation Effects in Semiconductors, Nice, 1978,* edited by J. H. Albany (Institute of Physics, Bristol, 1979).
[57]G. Guillot, A. Nouailhat, G. Vincent, M. Baldy, A. Chantre, Rev. Phys. Appl. 15, 679 (1980).
[58]G. Guillot, A. Nouailhat, G. Vincent, A. Chantre, and M. Baldy, in Radiation Effects in Semiconductors and Related Materials, Tbilissi, 1979 (unpublished).
[59]D. V. Lang, R. A. Logan, and L. C. Kimerling, Phys. Rev. B 15, 4874 (1977).
[60]A. Zylbersztejn, 2nd "Lund" International Conference on Deep Level Impurities in Semiconductors, Ste. Maxime, 1979 (unpublished).
[61]D. V. Lang, and L. C. Kimerling, Lattice Defects in Semiconductors, 1974 (Institute of Physics, Bristol, 1975), p. 581.
[62]D. Pons and S. Makram-Ebeid, J. Phys. F 40, 1161 (1979).
[63]D. Bois, Ph. D. thesis, Lyon, 1972, unpublished.
[64]A. L. Lin, E. M. Omel'Yanovskii, and R. H. Bube, J. Appl. Phys. 47, 1852 (1976).
[65]G. Lucovsky, Solid State Commun. 3, 299 (1965).
[66]A. A. Kopylov, and A. N. Pikhtin, Fiz. Tverd. Tela (Leningrad) 16, 1851 (1974) [Sov. Phys.–Solid. State 16, 1200 (1975)].
[67]U. Piekara, J. M. Langer, and B. Krukowska-Fuldl, Solid State Commun. 23, 583 (1977).
[68]M. Jaros, J. Phys. C 8, 2455 (1975).
[69]S. T. Pantelides and J. Bernhole, *International Conference on Radiation Effects in Semiconductors, Dubrovnik, 1976,* edited by N. B. Urli and J. W. Corbett

(Institute of Physics, Bristol, 1977), p. 465.
[70]H. G. Grimmeiss and L. Å. Lebedo, J. Phys. C 8, 2615 (1975).
[71]D. Bois and A. Chantre Rev. Phys. Appl. 15, 631 (1980).
[72]D. E. Aspnes, Phys. Rev. B 14, 5331 (1976).
[73]See, for example, J. C. Phillips, *Bonds and Bands in Semiconductors*, (Academic, New York, 1973), p. 118.
[74]W. J. Brown and J. S. Blakemore, J. Appl. Phys. 43, 2242 (1972).
[75]R. A. Craven and D. Finn, J. Appl. Phys. 50, 6334 (1979).